Original Articles

ETS-related gene (ERG) undermines genome stability in mouse prostate progenitors via Gsk3β dependent Nkx3.1 degradation

Marco Lorenzoni [a,1], Dario De Felice [a,3], Giulia Beccaceci [a], Giorgia Di Donato [a], Veronica Foletto [a], Sacha Genovesi [a], Arianna Bertossi [a], Francesco Cambuli [a,2], Francesca Lorenzin [a], Aurora Savino [b], Lidia Avalle [b], Alessia Cimadamore [c], Rodolfo Montironi [d], Veronica Weber [e], Francesco Giuseppe Carbone [e], Mattia Barbareschi [e], Francesca Demichelis [a], Alessandro Romanel [a], Valeria Poli [b], Giannino Del Sal [f], Marianna Kruithof-de Julio [g,h,i,j], Marco Gaspari [k,***], Alessandro Alaimo [a,**], Andrea Lunardi [a,*]

[a] *Department of Cellular, Computational and Integrative Biology-CIBIO, University of Trento, Trento, Italy*
[b] *Department of Molecular Biotechnology and Health Sciences, University of Torino, Torino, Italy*
[c] *Pathological Anatomy, School of Medicine, United Hospitals, Polytechnic University of the Marche Region, Ancona, Italy*
[d] *Molecular Medicine and Cell Therapy Foundation, Polytechnic University of the Marche Region, Via Tronto, 10, Ancona, Italy*
[e] *Unit of Surgical Pathology, Santa Chiara Hospital, Trento, Italy*
[f] *University of Trieste Department Life Sciences, ICGEB-Area Science Park Trieste, IFOM, Milan, Italy*
[g] *Urology Research Laboratory, Department for BioMedical Research DBMR, University of Bern, Bern, Switzerland*
[h] *Translational Organoid Resource CORE, Department for BioMedical Research, University of Bern, Bern, Switzerland*
[i] *Bern Center for Precision Medicine, Inselspital, University Hospital of Bern, Bern, Switzerland*
[j] *Department of Urology, Inselspital, University Hospital of Bern, Bern, Switzerland*
[k] *Research Centre for Advanced Biochemistry and Molecular Biology, Department of Experimental and Clinical Medicine, Magna Graecia University of Catanzaro, Catanzaro, Italy*

ARTICLE INFO

ABSTRACT

21q22.2–3 deletion is the most common copy number alteration in prostate cancer (PCa). The genomic rearrangement results in the androgen-dependent *de novo* expression of *ETS-related gene* (*ERG*) in prostate cancer cells, a condition promoting tumor progression to advanced stages of the disease.

Interestingly, ERG expression characterizes 5–30% of tumor precursor lesions – High Grade Prostatic Intraepithelial Neoplasia (HGPIN) - where its role remains unclear.

Here, by combining organoids technology with Click-chemistry coupled Mass Spectrometry, we demonstrate a prominent role of ERG in remodeling the protein secretome of prostate progenitors. Functionally, by lowering autocrine Wnt-4 signaling, ERG represses canonical Wnt pathway in prostate progenitors, and, in turn, promotes the accumulation of DNA double strand breaks via Gsk3β-dependent degradation of the tumor suppressor Nkx3.1. On the other hand, by shaping extracellular paracrine signals, ERG strengthens the pro-oxidative transcriptional signature of inflammatory macrophages, which we demonstrate to infiltrate pre-malignant ERG positive prostate lesions.

These findings highlight previously unrecognized functions of ERG in undermining adult prostate progenitor niche through cell autonomous and non-autonomous mechanisms. Overall, by supporting the survival and proliferation of prostate progenitors in the absence of growth stimuli and promoting the accumulation of DNA damage through destabilization of Nkx3.1, ERG could orchestrate the prelude to neoplastic transformation.

 * Corresponding author.
 ** Corresponding author.
 *** Corresponding author.
   E-mail addresses: gaspari@unicz.it (M. Gaspari), alessandro.alaimo@unitn.it (A. Alaimo), andrea.lunardi@unitn.it (A. Lunardi).
 [1] Present address: Cellular Immunology Unit, IRCCS Ospedale San Raffaele, Milan, Italy.
 [2] Present address: Molecular Pharmacology Program, Sloan Kettering Institute, Memorial Sloan Kettering Cancer Center, New York, NY, USA.
 [3] equally contributed.

1. Introduction

Prostate Cancer (PCa) is one of the most commonly diagnosed cancer in men [1]. In addition to aging, other risk factors are ethnicity (African American > Caucasian > Asian), family history (hereditary gene mutations of *BRCA2*), and lifestyle [2–5].

PCa is a slow-growing tumor commonly considered the natural progression of proliferative lesions characterized by clusters of cells invading the lumen of the prostatic ducts and accompanied by a reduced integrity of the basal epithelial compartment, namely High-Grade Prostatic Intra-epithelial Neoplasia (HGPIN) [6–8].

Among the molecular alterations described in PCa, unquestionably *Ets-related gene (ERG)* expression is the one with the highest incidence [9–11]. ERG is a member of the ETS-family of transcription factors, which is expressed in several tissues and involved in many different processes from cell proliferation and angiogenesis to cell differentiation and apoptosis [12,13].

The most common genomic rearrangement of *ERG* gene in prostate cells is a microdeletion in the q22 region of chromosome 21, which fuses exon 1 of the AR-responsive *Transmembrane Serine Protease 2 (TMPRSS2)* gene with exon 4 of *ERG* gene [14]. Since *TMRPSS2* Ex1 covers the promoter and 5′UTR region of the gene, the outcome of *TMPRSS2-ERG* fusion is not a chimeric protein but the *de-novo* AR-driven expression of a delta-40 amino-terminal truncated isoform of ERG in prostate epithelium [15–17]. *TMPRSS2-ERG* rearrangement is considered a very early event during prostate tumorigenesis and it is commonly identified in 5–30% of HGPIN prostate lesions [17–22]. However, several *in vivo* studies exploiting Genetically Engineered Mouse Models (GEMM) show that the expression of ERG in mouse prostate can, at most, induce benign lesions in the prostatic epithelium, but never malignant cell transformation and PCa [7,16,23–25]. These findings are further strengthened by the inability of ERG to trigger cell transformation in immortalized human prostate cell lines [23–26].

Even if the oncogenic role(s) of ERG in PCa have been functionally associated with invasive and metastatic tumor progression, the presence of genomic rearrangements driving ERG expression in 5–30% of HGPIN prostate lesions is at least counterintuitive and suggests possible critical role(s) of ERG in the very early stages of prostate tumorigenesis.

Here, by combining organoids technology and Click-chemistry approach coupled to Mass Spectrometry analyses, we demonstrate that ERG expression in prostate progenitors is functional to compromise normal prostate epithelium homeostasis, and characterize an ERG-dependent signature of secreted proteins with potential autocrine and paracrine roles in the generation of permissive conditions for tumor onset.

2. Material and Methods

2.1. Mouse husbandry and care

Wild-type C57BL/6J (JAX # 000664) mice were purchased from The Jackson Laboratory. Mice were housed in a certified Animal Facility in accordance with FELASA guidelines and recommendations, and were in compliance with the Directive 2010/63/UE and its Italian transposition D. L.vo 26/2014. All animal experiments were performed according to the European Communities Council Directive (2010/63/EU) and approved by the Italian Ministry of Health and the University of Trento Animal Welfare Committee (642/2017-PR) as conforming to the relevant regulatory standards.

2.2. Mouse prostate organoid cultures

Mouse prostate organoids (mPrOs) were generated from prostate glands collected from adult (6–12 months year-old) C57BL/6J wild-type males. Generation and establishment of mPrOs cultures were achieved as previously described [27–29]. Briefly, single cells or small clumps of cells were embedded in growth factor reduced Matrigel® (Corning, 356231) or BME-2® (AMSBIO, 3533) and plated as a 40 µl dome (1000–2000 cells/dome) in a 12-well cell culture plate (3 domes/well). Matrix domes were left to solidify and covered with ENRAD medium including: 50 ng/ml Egf (PeproTech, 315-09), 100 ng/ml Noggin (PeproTech 120-10C), 10% R-Spondin1 (conditioned medium), 200 nM A83-01 (Tocris, 2393) and 10 nM Dihydrotestosterone (DHT, Merck, 10300). Additionally, the medium was supplemented with 10 µM Y-27632 (Calbiochem, 146986-50-7; for 24–48 h after seeding) and with 10 nM ATRA (Merck R2625). Organoids were cultured in a standard tissue culture incubator. Medium was changed every 2–3 days and mPrOs growth was followed by stereoscopic analysis (Leica MZ16F). Organoids were passed once a week by recovering cells using 1 mg/ml Dispase II (ThermoFisher Sci.) and TrypLE (ThermoFisher Sci.), and mechanically dissociating into single cells or small clumps before replating/reseeding.

2.3. Generation of retroviral vectors and transduction of mPrOs

The retroviral vector pTGMP-ERG$_{M40}$ inducible for the expression of ERG was generated as previously described [26]. To produce retroviral particles, half-confluent HEK-293T cells in antibiotic-free DMEM medium were transfected with 10 µg of pTGMP-ERG$_{M40}$, 2.5 µg of the envelope pHDM-VSVG plasmid and 7.5 µg of the packaging pRetro-Gag-Pol plasmid supplemented with 50 µl of polyethylenimine (PEI, Sigma). Eight hours after transfection the medium was replaced with low FBS (3–5%) complete medium and, after 48 h, the supernatant was collected, filtrated, quantified [30] and, finally, stored at −80 °C. Stable mPrOs inducible for the expression of ERG were generated as described below. mPrOs cultures were mechanically dissociated into single cells and counted. The transduction was performed by spinoculation, mixing 2-3 x 10^5 cells, retroviral particles (0.3 RTU/reaction) and 4 µg/ml polybrene (Sigma, H9268) in a low adhesion 96-well plate. The sample was centrifuged for 1 h at 600 g. Cells were then gently resuspend, collected into a tube, and further incubated for 4–6 h at 37 °C. After this time, cells were pelleted and seeded as usual. Positive selection started 48 h after transduction adding 1 µg/mL puromycin (InvivoGen) to the medium and maintained for 2 weeks. The inducible expression of ERG was stimulated adding 1 µg/ml doxycycline (Sigma Aldrich) to the medium for at least 96 h. Stable mPrOs were tested and authenticated by Western blot and RT-qPCR for specific expression of ERG and its activity on known ERG-targeted genes [24,25].

2.4. Cell lines

RWPE-1 (#CRL-11609), LNCaP Fast Growing Clone (#CRL-1740) and VCaP (#CRL-2876) cell lines were purchased from the American Type Culture Collection (ATCC). LNCaP and 22Rv1 prostate cancer cell lines with inducible expression of ERG were generated in the Demichelis' laboratory with a vector kindly provided by David Rickman. Cells were cultured in a humidified incubator at 37 °C and 5% CO$_2$ and maintained according to manufacturer's instructions.

2.5. Quantitative RT-qPCR and end-point PCR

To collect RNA from mPrOs, 3 domes (1200–1500 cells/dome) were processed for each analyzed condition. The samples were mechanically dissociated with Dispase II, collected in a tube, incubated at 37 °C for 5 min, washed with 0.1% BSA in PBS and centrifuged (300 g, 5 min) before resuspending the cell pellet in the provided lysis buffer. RNA was extracted using the RNeasy Plus Micro kit (Qiagen, 74034) following the manufacturer's protocol. The concentration of the RNA was evaluated with a NanoDrop™ 2000c spectrophotometer (ThermoFisher Sci) while RNA quality was controlled via gel electrophoresis. Subsequently, RNA was retrotranscribed into cDNA using iScript™ cDNA synthesis Kit (Biorad, 1708891) according to the manufacturer's protocol.

Quantitative gene expression analysis was achieved through RT-qPCR exploiting the qPCRBIO SyGreen Mix (PCRBiosystems, PB20.14-05), according to the manufacturer instructions. Reaction mixes were prepared in final volumes of 10 μl, including 10 ng of cDNAs and gene-specific primers used at a final concentration of 200 nM. The experiments were performed in three or more technical replicates using the CFX96 qPCR thermocycler (BioRad) following standard protocols. Results were processed using the BioRad CFX Manager software (V. 3.1), while gene expression and statistical analysis were performed through GraphPad PRISM (V. 6.01).

End-point PCR amplification was carried out using Phusion Universal qPCR Kit (Life Tech, F566L), analyzing 50–100 ng of DNA on a C1000 Touch thermal cycler (Biorad). PCR products were loaded on agarose gels and separated by standard gel electrophoresis. DNA gels were imaged with an UV scanner (UVITEC). RT-qPCR and End-point PCR analyses were performed with at least 3 independent biological replicates, unless stated in the figure legend; representative data are shown. Primers are reported in Supplementary Table S1.

2.6. Subcellular fractionation and Western blotting

Organoids, usually collected from 6 domes (1200–1500 cells/dome), were washed in ice-cold PBS twice, pelleted and lysed for 30 min at 4 °C with RIPA buffer (50 mM Tris-HCl, pH 7.5, 150 mM NaCl, 1% Triton X-100, 1% sodium deoxycholate, 1% NP-40) supplemented with protease (Halt™ protease inhibitor cocktail, Life Tech, 87786) and phosphatase inhibitors (Phosphatase-Inhibitor-Mix II solution, Serva, 3905501). Cell fractionation was performed using NE-PER Nuclear and Cytoplasmic Extraction Kit (Life Tech, 78833) according to the manufacturer's instructions. Protein concentrations were quantified via BCA assay (Pierce™ BCA protein Assay Kit, ThermoFisher Sci. 23225). Lysates were resolved by SDS/PAGE and transferred to PVDF membrane (Amersham™ Hybond™, Fisher Scientific) using a wet electroblotting system (BioRad). The membranes were blocked with 5% non-fat dry milk or 5% BSA in TBS-T (50 mM Tris-HCl, pH 7.5, 150 mM NaCl, 0.1% Tween20) for 1 h at RT and then incubated with specific primary antibodies O/N at 4 °C (see below). After washes in TBS-T, membranes were incubated with an HRP-conjugated anti-rabbit (Cell Signaling, 7074) or HRP-linked anti-mouse (Cell Signaling, 7076) secondary antibody for 1 h at RT. Immunoreactive bands were detected using ECL LiteAblot plus kit A + B (Euroclone, GEHRPN2235) with an Alliance LD2 device and software (UVITEC). Western blots were performed in at least 3 independent biological replicates; representative data are shown. Primary antibodies used were: AR (Santa Cruz, sc-816), Cytokeratin 5 (Biolegend, 905501), Cytokeratin 8 (Abcam, ab53280), ERG (Abcam, ab133264), Fibrillarin (Abcam, ab4566), GAPDH (ThermoFisher Sci., MA515738), Nkx3.1 (Millipore, ab5983), PARP (Cell Signaling, 9542), phosphor-53BP1 (S^{25} Abcam, ab70323), phosphor-Atm (S^{1981}, Cell Signaling, 5883), phospho-H2AX (S^{139}, Abcam, ab26350), β-Actin (Sigma, A2228), β-Catenin (Abcam, ab32572), β-Tubulin (Santa Cruz, sc-5274).

2.7. Egf deprivation experiment

Two days before seeding, mPrOs were treated either with 1 μg/ml doxycycline-containing or mock medium. Following mechanical dissociation, 1200 cells were seeded in each dome and supplemented with EGF-deprived medium. After O/N incubation, 1 μg/ml doxycycline was added to treated samples, changing the medium every 2–3 days. At day 8, organoids were entirely reseeded in a new dome and doxycycline was added after 24 h, as previously described. Stereoscopic analysis (Leica MZ16F) was performed daily up to day 14, while viability assay was performed incubating organoids with 5 μM Calcein-AM (eBioscience, BMS65-0853-78) for 1 h and then analyzing them by fluorescent stereoscopic imaging.

2.8. Sample preparation for immunostaining

Organoids were seeded within ECM-like dome, let grow for 48 h and then treated with or without doxycycline during 72 h. Domes were then enzymatically disaggregated, and organoids were washed with 0.1% BSA in PBS and embedded in collagen-based matrix (Corning, 354249). After complete polymerization of the domes, complete medium was added to the cultures with the appropriate treatment and incubated for 24 h. Samples were washed with PBS and fixed with 4% PFA (Sigma Aldrich, P6148) for 5 h at RT, then collected into histological cassette and subjected to paraffin embedding. Prostate tissue was harvested, fixed and paraffin embedded using the same conditions. Formalin-fixed paraffin-embedded (FFPE) blocks were sectioned (5 μm–thick sections), collected onto glass slides and dried O/N at 37 °C.

2.9. Immunofluorescence

After deparaffinization and antigen retrieval, performed using a citrate-based buffer (pH 6.0) (Vector Lab, H3300), slides were permeabilized in blocking solution (5% FBS, 0.1% Triton X-100 in PBS) for 1 h at RT and then incubated O/N at 4 °C with primary antibodies. After washing, slides were incubated with Alexa Fluor conjugated secondary antibodies for 2 h and, before mounting, they were counterstained with Hoechst 33342 (Abcam, ab145597). All the images were acquired using an Axio Imager M2 (Zeiss), while image analysis and quantification was performed with ImageJ software (ImageJ 1.46r NIH). Immunofluorescence studies were performed in at least 3 independent biological replicates; representative data are shown. The following antibodies were used for immunofluorescence analysis: Ar (Rabbit, Santa Cruz, sc-816), Cytokeratin 5 (Chicken, Biolegend, 905901), Cytokeratin 8 (Rat, Merck, MABT329), ERG (Rabbit, Abcam, AB92513), β-Catenin (Rabbit, Abcam, ab32572), Ki67 (Rat, eBioscience, BMS14-5698-82), α-rabbit Alexa Fluor 488 (Donkey, Life Technologies, A21208), α-rat Alexa Fluor 594 (Donkey, Life Technologies, A21209), α-chicken Alexa Fluor 633 (Goat, Life Technologies, A21094).

2.10. Immunohistochemistry

Human prostate samples were retrieved from the archives of the Units of Surgical Pathology of the S. Chiara Hospital, Trento, Italy (protocol number 1946). Prostate TMA bearing 43 cases of HGPIN were generated at the Units of Surgical Pathology of the S. Chiara Hospital, while a TMA with 90 cases (60 cases of PCa and adjacent normal tissue + 30 cases of PCa) was purchased from US Biomax (HProA150PG01). Immunohistochemical analysis was performed at the Department of Histopathology (S. Chiara Hospital, Trento, Italy) using an automatic immunostainer (BOND-III platform, Leica Biosystems). Antigen retrieval was carried out with optimized BOND reagents (Bond epitope retrieval solution 1, Leica Biosystems) at pH 6 for 20 min. The following primary antibodies were used: ERG (Abcam, ab92513/1:500; Biocare, 9FY/1:400), CD68 (NCL-L-CD68, Leica Biosystems, 1:60), NKX3.1 (Biocare, D2Y1A/1:50), CK-5 (Novocastra, NCL-L-CK5/1:600), P63 (Leica, NCL-p63/1:50). BOND compact polymer detection solution (Leica Biosystems) was used for the detection. Slides were reviewed independently by two trained pathologists (M.B. and F.G.C.). Images were acquired using an Axio Imager M2 (Zeiss). This study was conducted according to the guidelines of the Declaration of Helsinki.

2.11. Flow cytometry analysis

Organoids were treated for 4 days with or without 1 μg/ml doxycycline and labeled with 10 μM 5-ethynyl-2′-deoxyuridine (EdU) for 3 h prior harvesting the samples. mPros were then collected, washed with 1% BSA in PBS, mechanically dissociated into single cells and filtered through a 30 μm cup strainer (BD Biosciences). Cells were pelleted and processed with the Click-iT™ Plus EdU Alexa Fluor™ 488 Flow

Cytometry Assay Kit (ThermoFisher Sci, C10632), following the manufacturer's instructions. DNA content staining was achieved through incubation with TO-PRO™-3 Iodide (Life Tech, T3695), before proceeding to the analysis. Flow cytometry was performed with a FACS CantoA flow cytometer (BD Biosciences), and data were analyzed with FlowJo v.10. For FACS analysis a CantoA flow cytometer (BD Biosciences) was used, and data were analyzed with FlowJo software (Treestar, V. 10.5.3).

2.12. Click-iT enrichment of secreted proteins

Organoids were seeded at the desired density, left to grow for 2 days, and then treated with or without doxycycline for 96 h. Before harvesting the medium, a step of Methionine depletion was performed culturing cells with Methionine-free medium for 2 h and then labeling samples O/N with Methionine-free organoid medium containing 0.1 mM L-azido-homoalanine (AHA) labeling agent (Jena Bioscience). Afterward, medium was recovered, centrifuged and clear supernatant was transferred in a new tube supplemented with protease and phosphatase inhibitors cocktail. At this stage, samples were stored at $-80\ °C$ or immediately processed for secreted, labeled protein enrichment. Enrichment protocol was based on Click-iT™ protein enrichment kit (ThermoFisher Sci, C10416) according to the optimized procedures described previously [31,32]. Collected medium was concentrated through centrifugation, mixed with Urea lysis buffer (8 M Urea, 200 mM Tris-HCl, 4% CHAPS, 1 M NaCl, pH 8) and then incubated with 1 mM Iodoacetamide dissolved in SDS washing buffer (100 mM Tris-HCl, 1% SDS, 250 mM NaCl, 5 mM EDTA pH 8) for 30 min at 20 °C, protected from light and with mild centrifugation (3000–4000 g). After that, the sample underwent cyclo-addition reaction incubating O/N at RT with alkyne matrix and catalyst solution. Reduction-alkylation steps were performed incubating the sample first with 10 mM DTT for 15 min at 70 °C plus additional 15 min at RT, and then with 40 mM Iodoacetamide for 30 min, protected from light. Subsequently, the resin was resuspended and extensively washed with SDS washing buffer, Tris-Urea washing buffer (8 M Urea, 100 mM Tris-HCl, pH 8), 20% isopropanol and 20% acetonitrile, respectively. The resin was then resuspended in digestion buffer (100 mM Tris-HCl, 2 mM CaCl$_2$, 10% acetonitrile, pH 8), pelleted and incubated with 2.5 ng/μl MS-grade trypsin (ThermoFisher Sci.) O/N at 37 °C with continuous rotation. After tryptic digestion, samples were centrifuged and the supernatant transferred in a new tube, while the resin was washed with water, pelleted and the supernatant added to the same tube to collect as much peptide as possible. Samples were then acidified with Trifluoroacetic acid and stored at $-80\ °C$ until MS analysis.

2.13. MS analysis

Tryptic peptide mix was first purified by reversed phase (C18) stage tip purification, as previously described [33] and eluted with a solution of 80% acetonitrile, 0.1% formic acid. The sample was vacuum dried and then resuspended with a solution of 2% acetonitrile, 0.1% formic acid.

LC-MS/MS analysis was performed with an EASY-LC 1000 coupled to a Q-Exactive mass spectrometer (ThermoFisher Scientific). The analytical nanoLC column is a pulled fused silica capillary, 75 μm i.d., in-house packed to a length of 12 cm with 3 μm C18 silica particles (Dr. Maisch GmbH). Peptide mixtures were loaded directly onto the analytical column. A binary gradient was used for peptide elution. Mobile phase A was composed by 2% acetonitrile/0.1% formic acid, whereas mobile phase B was 80% acetonitrile/0.1% formic acid. Gradient elution was achieved at 300 nl/min flow rate, ramped from 6% B to 40% B in 90 min, from 40% B to 100% B in 18 min, and remained at 100% B after additional 10 min. Mobile phase composition was finally brought to 0% B in 2 min. MS detection was performed on a quadrupole-orbitrap mass spectrometer Q-Exactive (ThermoFisher Scientific) operating in positive ion mode, with nanoelectrospray (nESI) potential at 1800 V applied on the column front-end via a tee piece. Data-dependent acquisition was

performed using a top-12 method with resolution (FWHM), AGC target and maximum injection time (ms) for full MS and MS/MS of, respectively, 70,000/35,000, 1e6/1e5, 50/120. Mass window for precursor ion isolation was 1.6 *m/z*, normalized collision energy was 25, and dynamic exclusion was 25 s. Injected amounts of samples varied from 4 to 8 μl, depending on peptide amount estimated from a preliminary injection. LC-MS/MS data analysis was conducted using the MaxQuant/Perseus software suite [34]. Label-free quantification was activated in MaxQuant, using default parameters except for the following: *i*) minimum peak length = 4; *ii*) mass accuracy = 3 ppm; *iii*); retention time window for match-between-runs options = 0.5 min (match-between-runs was set to "ON", with an alignment time window of 20 min). Data was searched on the "*Mus musculus* reference proteome", downloaded on August 11, 2018 (53,345 sequences). Label free quantification of proteins were based on the LFQ algorithm [35] and required a minimum of one unique/razor peptide associated to a specific identified protein.

The protein summary output table was loaded in Perseus for statistical and bioinformatic analysis. After removing hits from reverse and contaminants database and transforming LFQ intensity data in logarithmic space, proteins were filtered based on valid values (measurement present in at least 2 biological replicates of at least one sample group). Missing values were imputed using default parameters.

2.14. Protein network analysis

Analysis of protein-protein interaction network and pathway enrichment were achieved exploiting STRING V 11.0 web tool (https://string-db.org/) [36,37]. Proteins were identified by their unique Protein ID and were enclosed in the list only if identified in at least 3 different biological replicates with 2 or more "Unique peptides". Confidence score for the network ≥ 0.9.

2.15. Heat map

The heatmap was created using R and RStudio graphic software environment (R Core Team (2019). R: A language and environment for statistical computing. R Foundation for Statistical Computing, Vienna, Austria. URL https://www.R-project.org; RStudio Team (2018). RStudio: Integrated Development for R. RStudio, Inc., Boston, MA, URL http://www.rstudio.com). Data were visualized using the LFQ intensity value obtained from the MS analysis of each sample. The proteins were sorted based on the Fold Change value obtained comparing Mock and Doxy mPrOs-ERG and on the significance of the Fold Change evaluated.

2.16. TCGA RNAseq dataset analysis

Processed RNA-seq counts for TCGA PRAD dataset were downloaded from Recount2 data portal (PMID). Counts were scaled and transformed to RPKM values using the recount R package. Distribution of log2 (RPKM+1) values across normal and tumor samples were compared using two-sample Wilcoxon test statistics. Correlation between ERG and NKX3-1 transcript levels was calculated using Pearson correlation and regression line was computed fitting to a linear model. Provided visual inspection of the distribution of ERG transcript levels across TCGA PRAD tumor samples, patients presenting an evident over-expression of ERG transcript were selected using a threshold of log2(RPKM+1) equal to 3.

2.17. COMET assay

Mouse prostate organoids (mPrOs) were seeded at 2000 cells/dome in a 12-well plate with complete or Rspo-1 deprived culture medium for 6 days. ERG induction was performed for 96 h with doxycycline. After 6 days of culture, mPrOs were dissociated into single cells, harvested by centrifugation and re-suspended in ice-cold PBS. Cell counts were then normalized to 1×10^5 cells/mL. Comet Assay was performed following the manufacturer instructions (Abcam, ab238544). Briefly, suspended

cells were combined with Comet Agarose at 1/10 ratio (v/v) and transferred (75 μL) on the top of the Comet Agarose Base Layer. The agarose-cell mixture was then dropped onto slides and let solidify at 4 °C in the dark for 15 min before immersion in COMET assay Lysis Buffer at 4° in the dark for 45 min. Excess buffer was then removed and slides were submerged in freshly prepared Alkaline Electrophoresis Solution at 4 °C in the dark for 30 min. When performed in Alkaline Solution, the COMET assay measures relative levels of DNA single and double-strand break fragmentation. Gel electrophoresis was then performed at 20 V (300 mA) for 25 min. Slides were then washed twice by immersion in pre-chilled dH$_2$O. Slides were then fixed in 70% ethanol for 5 min. Following air drying of the agarose, slides were stained with Vista Green DNA Dye and images were collected with a 10× objective lens. COMET tail moments were then assessed using COMETscore.v2.0 (TriTek Corp., Sumerduck, VA) image processing software and OpenComet plugin (FIJI – ImageJ) with greater than 100 cells analyzed per condition. Data is reported as tail moment, which assesses the fluorescence intensity in the tail relative to the head while accounting for the relative area of both dipoles.

2.18. Macrophages

Primary mouse Bone Marrow Derived Macrophages (BMDMs) were obtained from femurs of WT C57B/6J mice (3–6 months of age). Specifically, BM was flushed out with PBS, broke down by pipetting and gently pelleted. Cells were then resuspended in ACK lysis buffer (Life Tech., A1049201), incubated at room temperature for 5 min, diluted with PBS and gently pelleted again to remove lysis buffer. Cells were then resuspended in RPMI culture medium (10% Heat-Inactivated FBS, 1 mM L-glutamine, 1% Pen/Strep), counted and seeded at about 2 million cells per well of a 6 well plate in culture medium supplemented with 10 ng/ml recombinant M-CSF (SinoBiological, #51112-MNAH). Macrophages were cultured for 7 days, replacing medium every 2–3 days, in presence of M-CSF. To induce M1 macrophage polarization, cells are cultured for 48 h with 0.1 μg/ml Lipopolysaccharide (LPS; Sigma, #L4516) and 50 ng/ml recombinant IFNg (SinoBiological, #50709-MNAH). Interleukin 4 (10 ng/mL; SinoBiological, #51084-MNAE) and interleukin 13 (10 ng/mL; SinoBiological, #50225-MNAH) were used to induce M2 polarization.

For the analysis of mPrOs influence, samples were treated with 50% mPrOs conditioned medium, or unconditioned control, for 48 h while adding the indicated polarization cocktail to the culture conditions. At the end of the incubation cell were lysed in the provided lysis buffe and RNA was extracted using the RNeasy Plus Micro kit (Qiagen, 74034) following manufacturer's protocol.

RNA was then processed as described in the previous paragraph for RT-qPCR analysis of selected targets.

2.19. Statistical analysis

GraphPad Prism 6 software (GraphPad Software Inc.) was used for all statistical analyses applied to the experimental data. Student *t*-test for unpaired or paired (relative to Fig. 5) data (two-tailed) was used to test the probability of significant differences between two groups of samples. Data are presented as mean ± SD of at least three independent experiments, unless stated in the figure legend. Statistical significance is presented as * $p \leq 0.05$, ** $p \leq 0.01$, *** $p \leq 0.001$. Significant differences in the amount of secreted proteins across different conditions were assessed for significance according to the Benjamini-Hochberg method with a FDR <0.2. An additional fold-change cutoff for biological significance was applied (either Fold Changes FC > 2 or FC < 0.5).

3. Results

### 3.1. ERG influences cell lineage and Egf dependency of mouse prostate progenitors

The recent development of 3D prostate organoids cultures from mouse and human adult prostate tissue [28,29,38,39] has opened a new window of opportunity for the study of prostate physiology, tissue homeostasis and tumorigenesis. Taking advantage of this new knowledge, we established a biobank of mouse prostate organoid (mPrO) lines derived from wild type and genetically engineered mice of different strains, by pooling the different prostate lobes (ventral, dorsolateral and anterior) or taking them separately [27].

In order to genetically engineer wild type mPrOs with a doxycycline inducible ERG expression vector system, ERG cDNA was cloned from VCaP cells, a human PCa cell line that carries the *TMPRSS2-ERG* rearrangement and expresses a shorter form of ERG starting from methionine 40 (ERG$_{M40}$), and inserted through enzymatic restriction into the retroviral pTGMP-rtTA3 plasmid downstream the TRE-CMV promoter element (pTGMP-ERG$_{M40}$) [26]. Wild type prostate organoids were generated by pooling together the three prostate lobes of C57BL/6J mice (Fig. 1) and transduced with pTGMP-ERG$_{M40}$ bearing viral particles (Supplementary Fig. S1A). mPrOs-ERG$_{M40}$ were grown for 4 passages (one month) in presence of puromycin to stabilize the line, then RT-qPCR and Western blot analyses were run on wild type mPrOs and mPrOs-ERG$_{M40}$ treated or not with 1 μg/ml doxycycline for 96 h. ERG$_{M40}$ was robustly expressed in the mPrOs-ERG$_{M40}$ induced with doxycycline, although a slight amount of ERG$_{M40}$ mRNA was also noted in non-induced mPrOs-ERG$_{M40}$ (Fig. 2A–B). Nevertheless, immunodetection analyses and gene expression studies on specific ERG-targeted genes (*Plau, Mmp3, Fam25c* and *Smim6*) [24,25] showed ERG$_{M40}$ protein and the expected transcriptional response exclusively in the mPrOs-ERG$_{M40}$ treated with doxycycline (Fig. 2C–D).

Immunofluorescence staining for Krt 5 and Krt 8 markers pointed out the diffusion of Krt 8 signal into the basal cell compartment in doxycycline treated mPrOs-ERG$_{M40}$ (Fig. 2E and Supplementary Fig. S1B), while immunoblot and RT-qPCR studies showed a significant increase in the expression of Krt 8 at both mRNA and protein levels in mPrOs-ERG$_{M40}$ treated with doxycycline, which was accompanied by concomitant reduction of Krt 5 levels (Fig. 2F–G). We then analyzed the proliferation rate of wild type mPrOs and mPrOs-ERG$_{M40}$ either with or without doxycycline administration. Quantification of Ki67+ cells in the four different conditions showed a significant reduction in the number of proliferating cells in ERG$_{M40}$ expressing mPrOs (Fig. 2H–I). To carefully investigate the effect of ERG$_{M40}$ on cell cycle, wild type and ERG$_{M40}$ mPrOs were treated with 5-ethynyl-2′-deoxyuridine (EdU) and analyzed by flow cytometry. EdU incorporation did not show any significant alteration in the fraction of cells in active DNA replication in the four different conditions (Fig. 2J). Since Ki67 discriminates proliferating cells regardless of the phase of the cell cycle in which they are (G1, S, G2 and M) from those in G0, we investigated the consequence of prolonging ERG$_{M40}$ expression in mPrOs. At the end of the first week, doxycycline-treated mPrOs-ERG$_{M40}$ culture showed a barely detectable reduction of organoids size and number. After reseeding, such differences became much more pronounced at the end of the second week, thus confirming a mild but consistent effect of ERG$_{M40}$ in lowering the proliferative potential of mouse prostate progenitor cells (Supplementary Fig. S2).

Besides the deregulation of mechanisms controlling cell proliferation and differentiation, a further important feature that increases the risk of a neoplastic transformation is the ability of pre-malignant cells to grow under nutrients and growth factors restrictions.

To test this eventuality, wild type and ERG$_{M40}$ mPrOs were cultured with or without doxycycline, and in the presence or absence of Epithelial Growth Factor (EGF) for up to two weeks. Compared to normal conditions (EGF 50 ng/ml), EGF withdrawal precludes the growth of wild type mPrOs, as well as of mock ERG$_{M40}$ organoids. Contrarily, doxycycline-
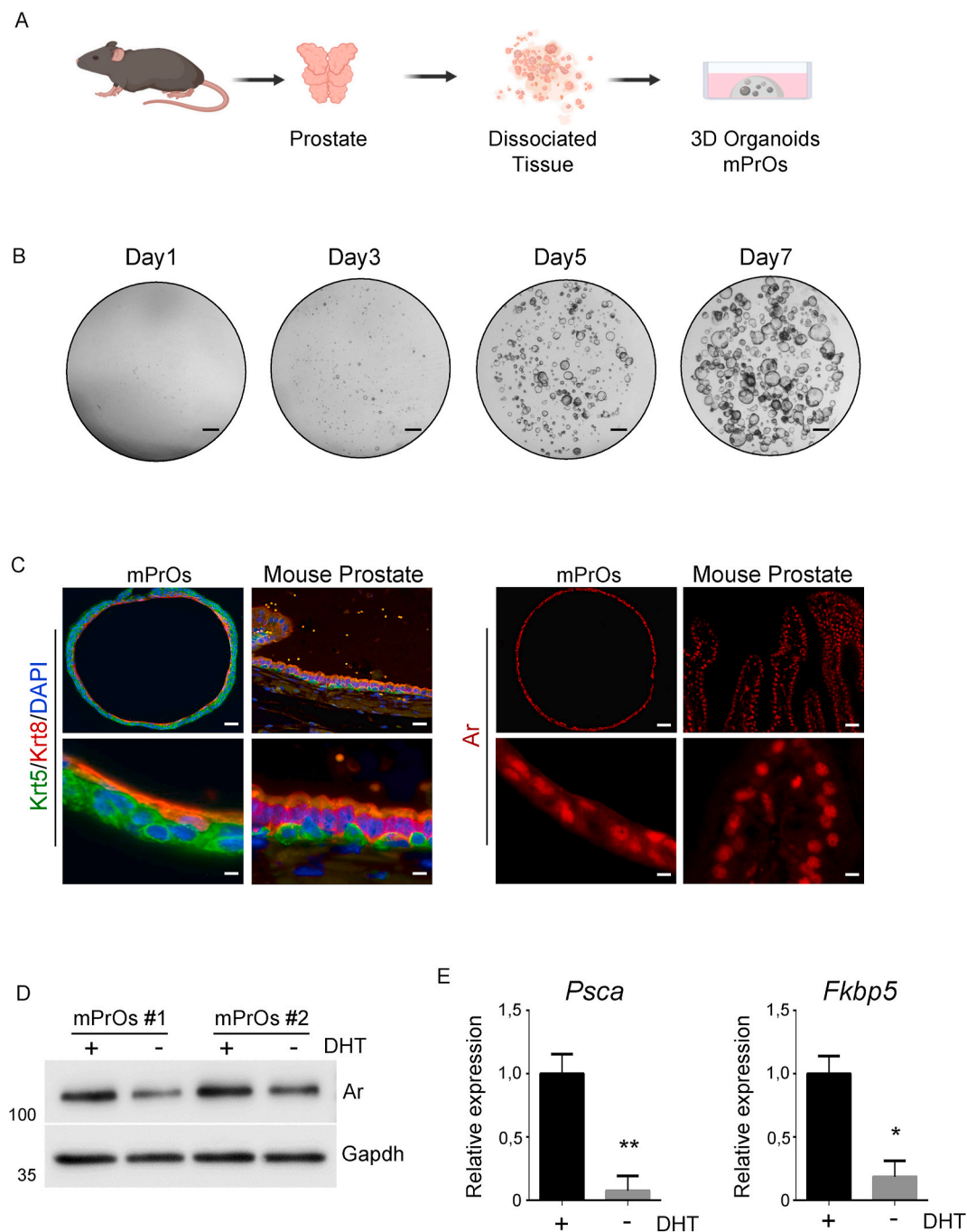
Fig. 1. *Establishing mouse Prostate Organoids Culture*
A. Scheme showing prostate organoids derivation from wild type mouse adult prostate tissue. B. Organoid culture growth within ECM-like domes. Scale bar: 200 μm
C. Immunofluorescent analysis of basal (Krt 5) and luminal (Krt 8; Ar) markers in mouse prostate organoids (left panels) and adult prostate tissue (right panels). DAPI was used for nuclear staining. Lower panels show inset magnifications of specified area. Scale bars: 50 μm upper panels; 10 μm lower panels.D. Western blot analysis of Ar in mouse prostate organoids with or without dihydrotestosterone (DHT).E. Expression levels of Ar target genes in mouse prostate organoids cultured with or without DHT.Statistical analyses were performed on at least n = 3 independent biological replicates. * = p-value <0.05; ** = p-value <0.01.

treated mPrOs-ERG$_{M40}$ survive and, albeit slowly, form vital 3D organoids, as observed with calcein labelling (Fig. 2K and Supplementary Fig. S2B).

3.2. ERG expression in mPrOs alters the secreted proteome

Click-chemistry coupled with Mass Spectrometry (Click-MS) is an efficient method for the study of secreted proteins [31,32].
Wild type mPrOs were exposed to AHA for 16 h, then supernatants were collected and processed according to the Click-MS protocol (Fig. 3A and Supplementary Fig. S3; see also Material and Methods). Four independent biological replicates were analyzed over six months and more than 200 proteins per replicate were unequivocally identified by at least two unique peptides. Of note, 172 proteins were recurrently identified in all the 4 biological replicates (Fig. 3B and Supplementary Table S2), thus demonstrating the robustness of the Click-MS approach and the remarkable stability of wild type mPrOs cultures over time (Cambuli et al., *submitted*; Karthaus et al., 2014). Importantly, a
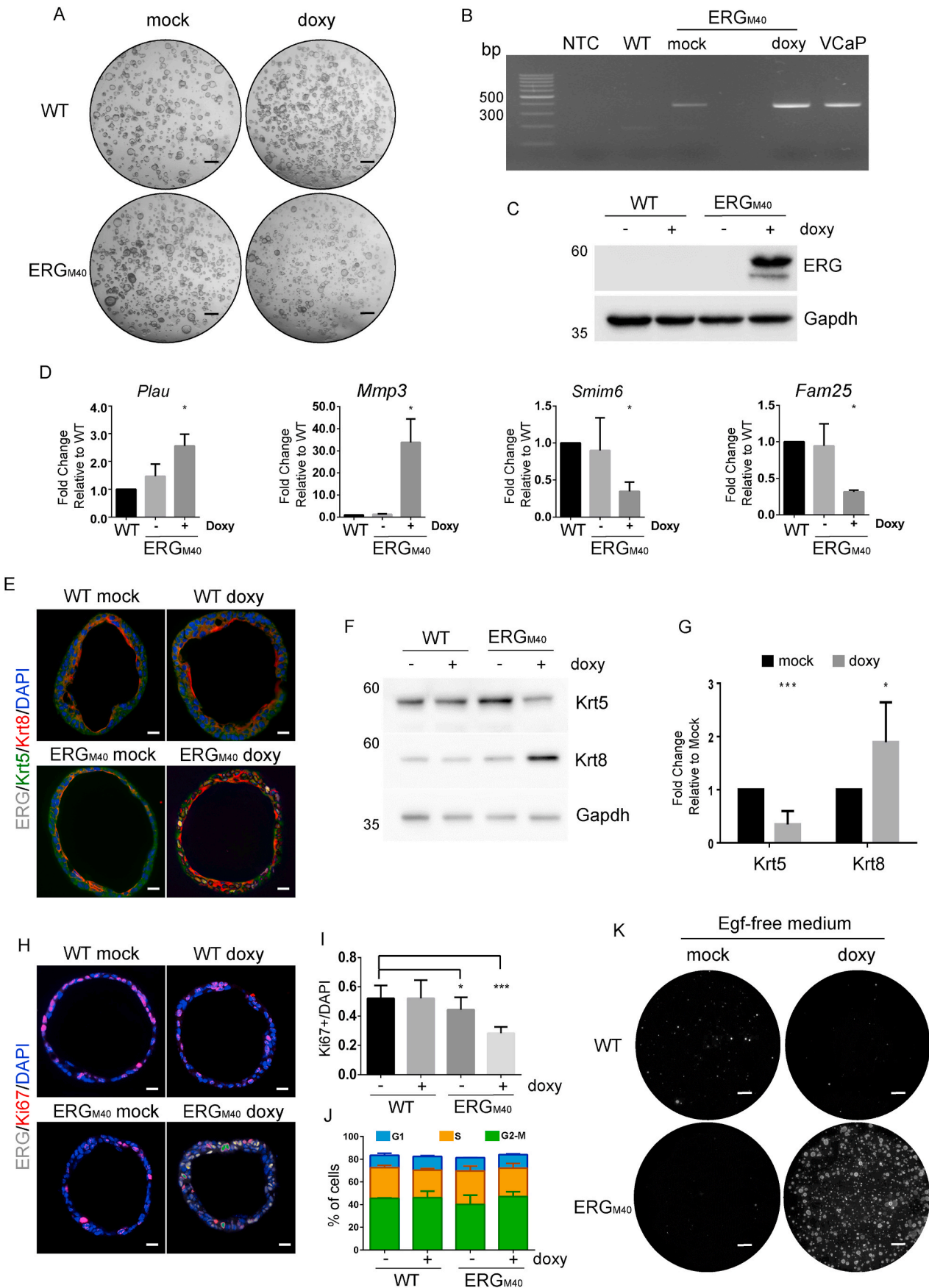
Fig. 2. *Characterization of mPrOs-ERG$_{M40}$*

A. Phenotypic analysis of mPrOs-WT and mPrOs-ERG$_{M40}$ treated for 96 h with doxycycline (doxy) or left untreated (mock). Scale bars: 200 μm B. *ERG* expression in mPrOs. cDNA from VCAP cell line was used as positive control. C. Immunoblot with ERG-specific antibody of protein extracts from mPrOs-WT and mPrOs-ERG$_{M40}$ treated with doxycycline for 96 h or left untreated. Gapdh was used as loading control. D. RT-qPCR analysis of known ERG-targeted genes in mPrOs-ERG$_{M40}$ after treatment with or without doxycycline for 96 h mPrOs-WT were used as reference. E. Immunofluorescence analysis of ERG, Krt 8 and Krt 5 in mPrOs-WT and mPrOs-ERG$_{M40}$ treated with doxycycline for 96 h (doxy) or left untreated (mock). DAPI was used for nuclear staining. Scale bars: 50 μm. F. Immunoblot analysis of Krt 8 and Krt 5 expression in mPrOs-WT and mPrOs-ERG$_{M40}$ treated with doxycycline for 96 h or left untreated. Gapdh was used as loading control. G. RT-qPCR analysis of *Krt 5* and *Krt 8* expression in mPrOs-ERG$_{M40}$ treated with doxycycline (doxy) for 96 h or left untreated (mock). H. Immunofluorescence analysis of ERG and Ki67 expression mPrOs-WT and mPrOs-ERG$_{M40}$ treated with doxycycline for 96 h or left untreated. DAPI was used for nuclear staining. Scale bars: 50 μm. I. Percentage of Ki67+ cells in mPrOs-WT and mPrOs-ERG$_{M40}$ treated with doxycycline for 96 h or left untreated. Quantification was performed on sections of n = 10 organoids per condition (WT mock = 1.396; WT doxy = 1.181; ERG$_{M40}$ = 1.380; ERG$_{M40}$ doxy = 1.345 total cells counted).J. Analysis of cell cycle progression of mPrOs-WT and mPrOs-ERG$_{M40}$ treated with doxycycline for 96 h or left untreated. Histogram shows the quantification of the FACS analysis.K. Phenotypic analysis of mPrOs-WT and mPrOs-ERG$_{M40}$ cultured with Egf-free medium for up to two weeks. Doxycycline was maintained throughout the duration of the experiment. Fluorescent images were acquired following 1 h incubation with 5 μM calcein. Scale bars: 200 μm. Statistical analyses were performed on at least n = 3 independent biological replicates. * = p-value <0.05; ** = p-value <0.01; *** = p-value <0.001.

literature-based study of the identified proteins defined more than 20% of the hits as already known prostate secreted factors (*e.g.* Activin A, VEGF, GDF15, MST1, Clusterin, SBSN, IGFBP3, LCN2, SPON2, LTF, Supplementary Table S2) [40–42], thus further reinforcing the thesis that mPrOs can be an interesting new biological system to model and study prostate tissue homeostasis and disease. Proteins that have been identified in at least 3 out of 4 replicates by at least two unique peptides were included in ontology and protein network studies. Ontology classification performed with DAVID software V. 6.8 [43,44] showed a significant enrichment of GO terms associated with the extracellular space, thus demonstrating the robustness of our approach (Supplementary Table S3). STRING software V 11.0 [37] was used to investigate protein networks. Data generated from this analysis includes a total number of 216 proteins and shows 3 highly connected cores of elements: Extracellular matrix (ECM) organization (MMU-1474244), Regulation of IGF transport and uptake (MMU-381426), and Innate immune system (MMU-168256) (Fig. 3C–D and Supplementary Table S4). Because of the high level of confidence (interaction score ≥0.9) imposed to the analysis, almost 40% of proteins are not connected with any other element meaning that other interesting networks could potentially emerge by lowering the stringency.

Click-it/MS studies were then extended to ERG$_{M40}$ mPrOs. Organoids were treated with doxycycline (1 μg/ml), or left untreated (mock), for 96 h before AHA labelling. Four independent biological replicates were analyzed for each condition. Approximately 200 proteins per sample were identified (by at least two unique peptides), of which 150, 154 and 142 were recurrently found in all the 4 replicates of wild type mPrOs treated with doxycycline (WT doxy), mPrOs-ERG$_{M40}$ left untreated (ERG mock), and mPrOs-ERG$_{M40}$ treated with doxycycline (ERG doxy), respectively (Fig. 3E–F, Supplementary Figs. S4A–B and Supplementary Table S5). Then, the number of shared proteins among the 4 different conditions was analyzed. To increase the coverage of our study, we included in this analysis proteins identified by minimum 2 unique peptides in at least 3 replicates out of 4. As shown by the Venn diagram in Fig. 3F, the largest fraction of proteins (n = 137) was identified in all the 4 different conditions, while some others resulted exclusively detected in (n = 17), or not detected (n = 20), in the supernatant of doxycycline-induced mPrOs-ERG$_{M40}$. MaxQuant label-free quantification, based on LFQ algorithm and exploiting the MaxQuant/Perseus software suite [34,35] was used to estimate significant differences in the amount of the secreted proteins between mPrOs expressing ERG$_{M40}$ and those that do not. The heatmap, obtained by plotting the intensity values calculated for every single identified protein in the 4 replicates of the 4 conditions (Fig. 3G), highlights a signature of secreted proteins whose relative amount in the secretome changes according to ERG$_{M40}$ expression (Supplementary Table S6). Thirty-seven proteins show significant differences >2 folds (either Fold Change FC > 2 or FC < 0.5, with significance assessed by the Benjamini-Hochberg method, FDR <0.2) in the doxycycline-induced mPrOs-ERGM40 compared to all other conditions. Among these, Lcn2, C16orf89, Spon2, Spink5 and Ctla2α are the

proteins that mark the most the mPrOs-ERG$_{M40}$ secretome, while Sbsn and Wnt-4 appear substantially underrepresented (Fig. 3H–I). Of note, RT-qPCR analysis demonstrates a significant change in the expression of these genes in doxycycline treated mPrOs-ERG$_{M40}$ (Fig. 3J), suggesting transcriptional control by ERG$_{M40}$.

3.3. ERG modulates canonical Wnt signaling in prostate progenitors promoting double strand breaks accumulation via Gsk3β-dependent Nkx3.1 degradation
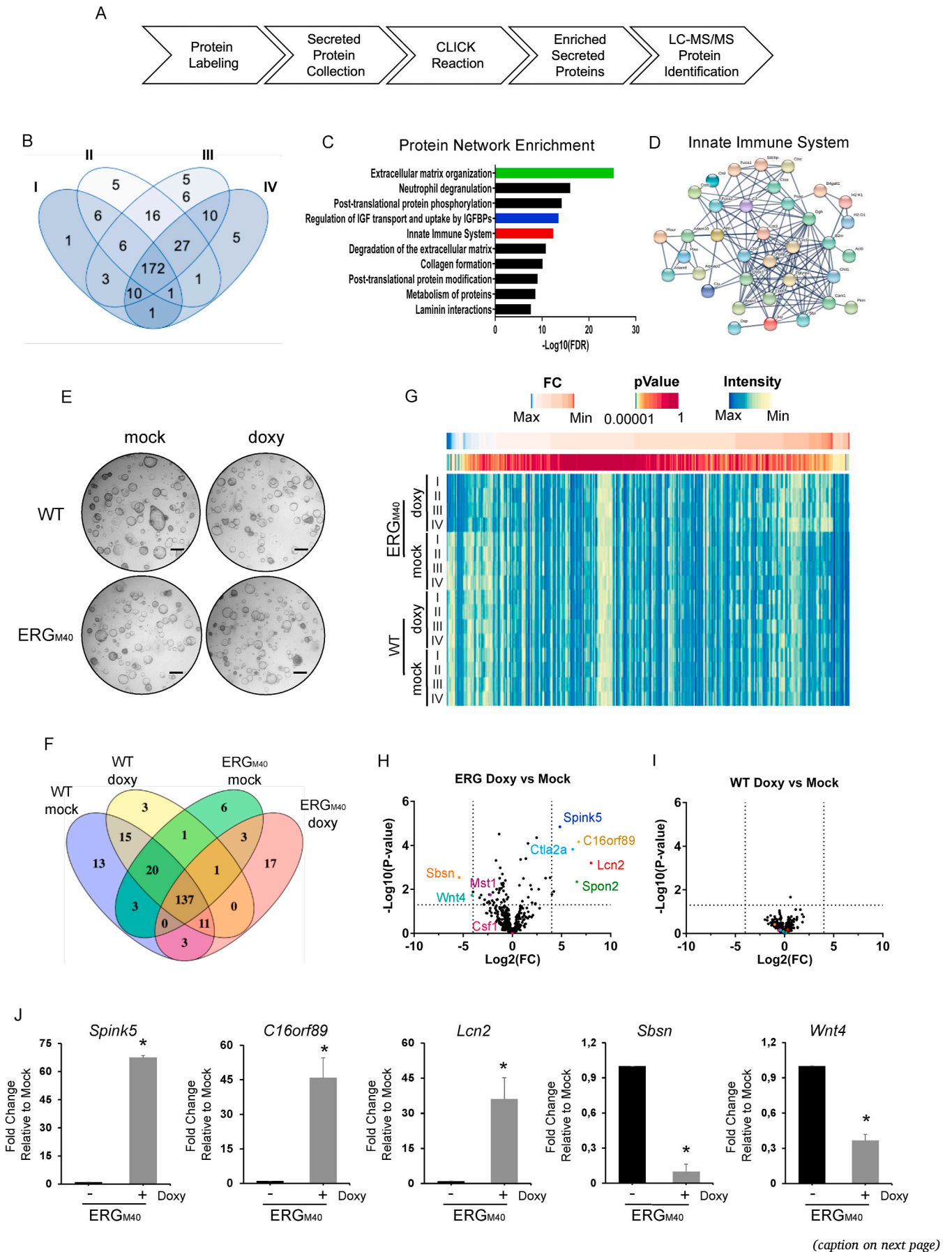
Transcriptional profile data of wild type mPrOs (Cambuli et al., *submitted*) shows robust expression of all key-components of the canonical Wnt pathway, included several Wnt ligands (Wnt-4, -7a and -7b, -9a, and −10a) (Supplementary Fig. S5A). However, our proteomic studies identify only Wnt-4 in the supernatant of mPrOs. Of note, Wnt-4 and Rspo1 have been shown to coordinate early gonads formations in both male and female mouse embryos [45]. Decreased Wnt-4 secretion in ERG + organoids accompanied a substantial reduction of nuclear β-Catenin (Fig. 4A) and the transcriptional downregulation of canonical β-Catenin targeted genes, included, unexpectedly, *Lgr4,* the most expressed Rspo1 receptor in mouse prostate organoids (Fig. 4B). A similar molecular signature was obtained in wild type organoids following Rspo1 deprivation (Supplementary Figs. S5B–C), while combination of ERG induction and Rspo1 depletion almost abrogated β-Catenin expression in organoids (Fig. 4C–E). Of note, β-Catenin preferentially marks the basal (Krt 8 negative) cells of wild type organoids (Fig. 4E and Supplementary Fig. S5D), and its reduction in ERG + mPrOs seems to go hand in hand with expansion of the Krt 8 compartment (Fig. 4E and Supplementary Fig. S5D).

During prostate development, canonical Wnt-signaling has been demonstrated promoting the expression of *Nkx3.1*, a pioneering transcription factor essential in the initial commitment and terminal differentiation of the luminal compartment of the gland epithelium [46, 47].

The amount of *Nkx3.1* transcript is relatively low in mPrOs (Cambuli et al., *submitted*), and further declines in the absence of Rspo1 (Fig. 5A, left panel). ERG expression substantially increases the levels of *Nkx3.1* RNA in mPrOs (Fig. 5A, middle panel), although the effect is less pronounced in the absence of Rspo1 (Fig. 5A, right panel).

Regardless of the amount of transcript, NKX3.1 protein can be tuned via post-transcriptional mechanisms that regulate protein stability in prostate cells [48–52]. Phosphorylation of Thr-89 and Thr-96 residues in the N-terminal PEST domain, as well as of Ser-185, Ser-186, Ser-195 and Ser-196 residues in the carboxy-terminal, of the protein drives ubiquitination and proteasome degradation of NKX3.1 under normal and stressed conditions (*e.g.* inflammation), respectively. However, little is known regarding signaling pathways and kinases involved in the control of NKX3.1 stability [53]. Interestingly, either ERG expression or Rspo1 deprivation alone does not change the amount of Nkx3.1 protein in mPrOs, which is instead severely reduced by the combination of both

A

Protein Labeling → Secreted Protein Collection → CLICK Reaction → Enriched Secreted Proteins → LC-MS/MS Protein Identification

B

C

Protein Network Enrichment

- Extracellular matrix organization
- Neutrophil degranulation
- Post-translational protein phosphorylation
- Regulation of IGF transport and uptake by IGFBPs
- Innate Immune System
- Degradation of the extracellular matrix
- Collagen formation
- Post-translational protein modification
- Metabolism of proteins
- Laminin interactions

-Log10(FDR)

D

Innate Immune System

E

G

F

H

ERG Doxy vs Mock

I

WT Doxy vs Mock

J

(caption on next page)

Fig. 3. *Mass spectrometry analysis of secreted proteins*

A. Schematic representation of Click-it chemistry coupled Mass Spectrometry approach. B. Venn diagram showing the number of secreted proteins identified from mPrOs-WT (n = 4). C. Histogram showing the top 10 enriched pathways identified by STRING (V 11.0). D. Protein-Protein interaction network obtained with STRING (V 11.0) generated starting from the secreted proteins included in the pathway "Innate Immune System", highlighted in C. E. mPrOs-WT and mPrOs-ERG$_{M40}$ organoids treated with doxycycline for 96 h or left untreated, labeled O/N with AHA. Scale bar: 200 μm. F. Venn diagrams showing the degree of shared and unique proteins in the four conditions described in E. Identified proteins were associated to a specific condition if identified with at least 2 "Unique peptides" in at least 3 biological replicates (n = 4). G. Heatmap showing LFQ intensity values for each protein in each analyzed sample. H. Volcano plot showing proteins differentially secreted by mPrOs-ERG$_{M40}$ treated with doxycycline or left untreated. Colored spots are associated to proteins of interest. I. Volcano plot comparing mPrOs-WT treated with doxycycline or left. Colored spots code as in H. J. Expression analysis of the genes encoding the five most deregulated proteins in mPrOs-ERG$_{M40}$. Statistical analyses were performed on at least n = 3 independent biological replicates. * = p-value <0.01.
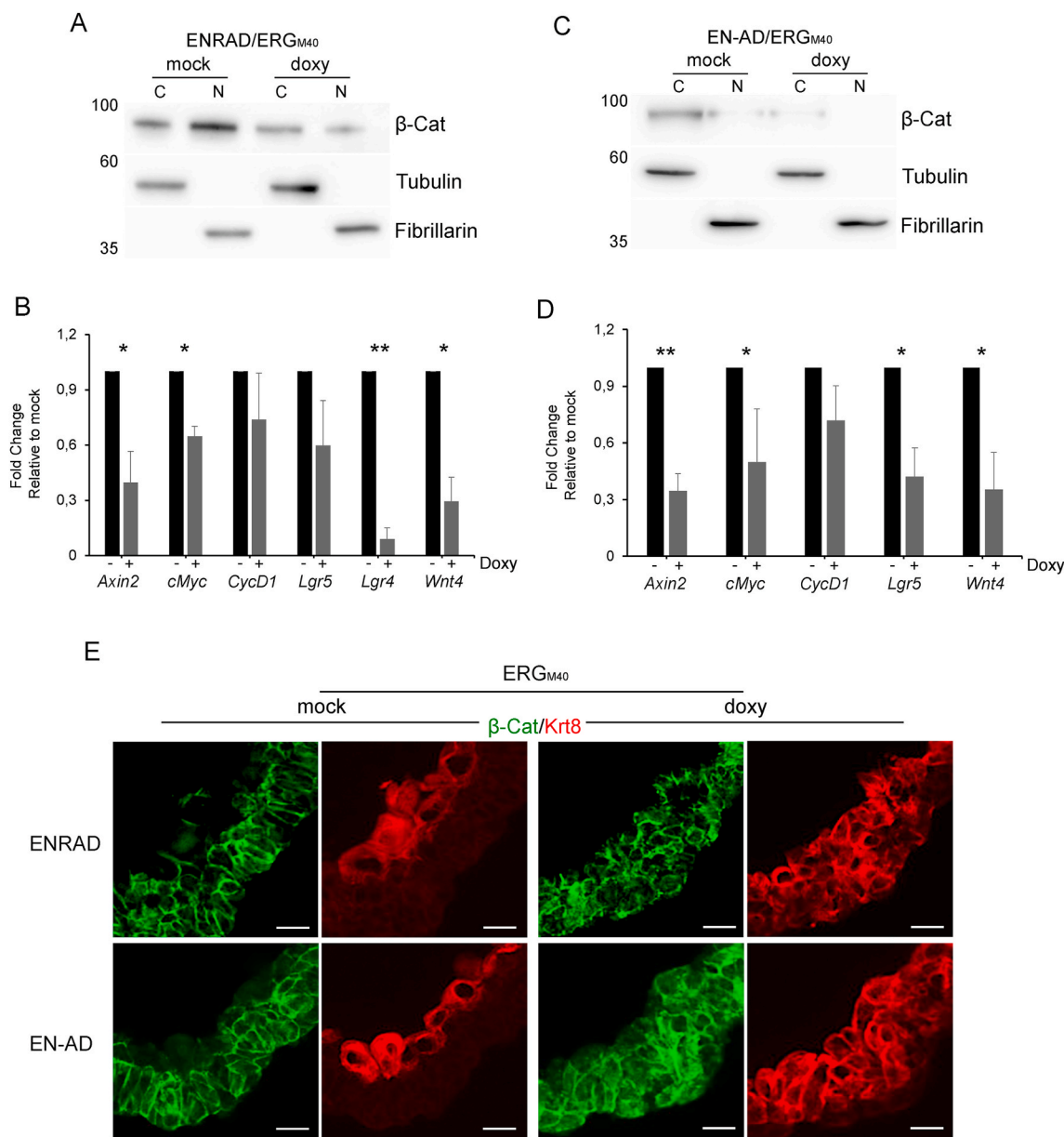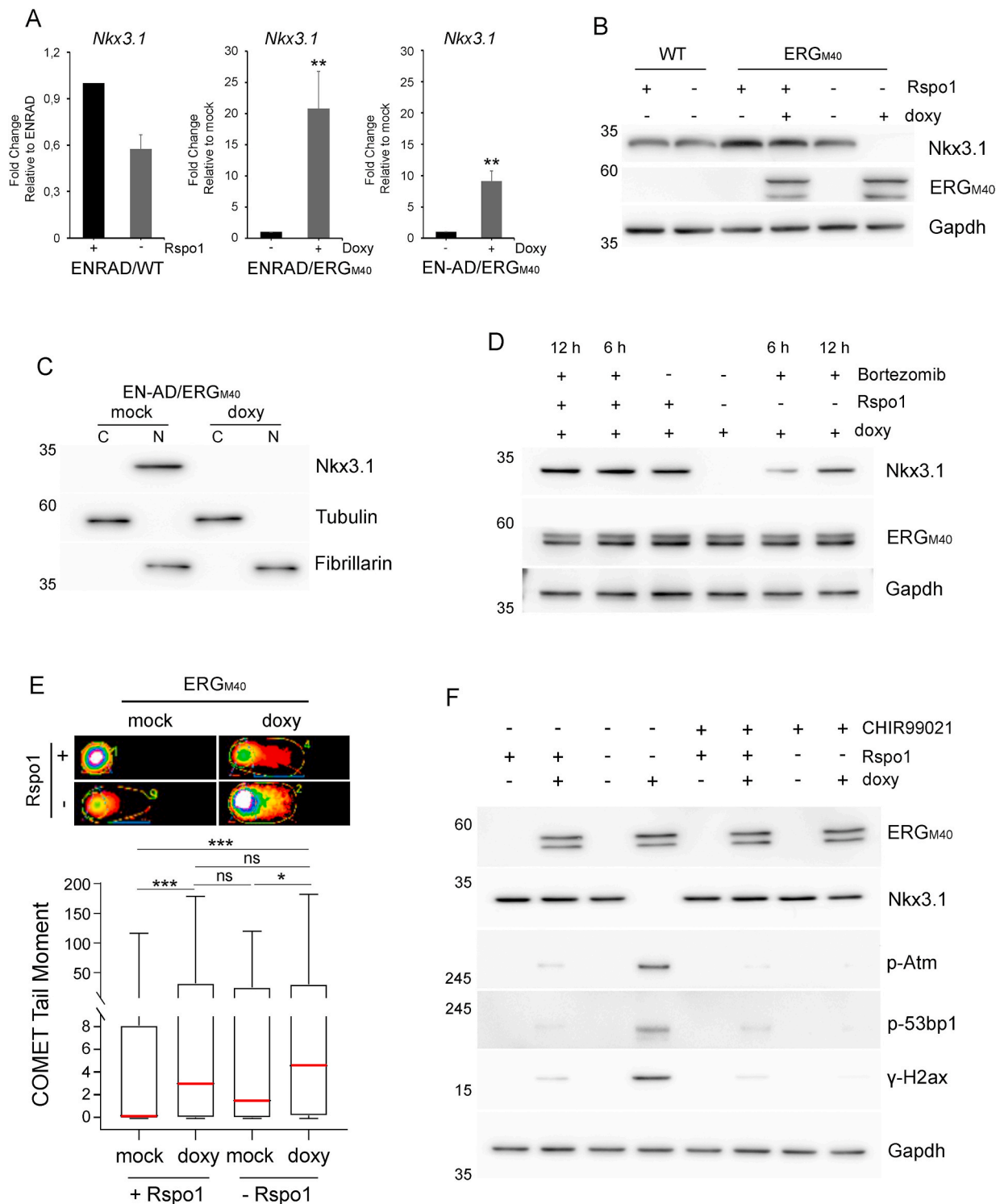

Fig. 4. *ERG$_{M40}$ inhibition of canonical Wnt pathway*

A. Immunoblot analysis of cytosolic and nuclear levels of β-Catenin in mPrOs-ERG$_{M40}$ treated with doxycycline for 96 h or left untreated. B. RT-qPCR analysis of canonical Wnt pathway targeted genes in mPrOs described in A. C. Immunoblot analysis of cytosolic and nuclear b-Catenin in mPrOs-ERG$_{M40}$ cultured without Rspo1 and treated with doxycycline for 96 h or left untreated. D. RT-qPCR analysis of canonical Wnt pathway targeted genes in mPrOs described in C. E. Immunofluorescence analysis for β-Catenin (green) and Krt8 (red) in mPrOs-ERG$_{M40}$ treated with doxycycline for 96 h or left untreated, cultured in presence (ENRAD) or absence (EN-AD) of Rspo1. (Scale bar: 10 μm). (For interpretation of the references to colour in this figure legend, the reader is referred to the Web version of this article.)

(Fig. 5B–C and Supplementary Fig. S5F). Bortezomib administration restores Nkx3.1 protein levels in ERG + mPrOs cultured without Rspo1, thus demonstrating proteosome involvement in proteolytic degradation of Nkx3.1 (Fig. 5D). Of note, Nkx3.1 loss has minor effect on the luminal drift triggered by ERG in prostate organoids (Supplementary Fig. S5G). Decreased levels of NKX3.1 protein are frequently described in PCa

Fig. 5. *ERG$_{M40}$ dependent mechanisms of genomic instability*

A. Nkx3.1 expression in mPrOs-WT cultured with or without Rspo1 (left), in mPrOs-ERG$_{M40}$ cultured with or without doxycycline (middle), and in mPrOs-ERG$_{M40}$ treated with doxycycline for 96 h or left untreated and cultured without Rspo1 (right). T-test, * = p value < 0.05; ** = p-value <0.01; *** = p-value <0.001.B. Immunoblot analysis of Nkx3.1 in wild type and ERG$_{M40}$ mPrOs cultured with or without Rspo1. mPrOs-ERG$_{M40}$ were treated with doxycycline for 96 h or left untreated.C. Immunoblot analysis of cytosolic and nuclear levels of Nkx3.1 in mPrOs-ERG$_{M40}$ treated with doxycycline for 96 h or left untreated and cultured without Rspo1.D. Immunoblot analysis of Nkx3.1 and ERG$_{M40}$ in mPrOs-ERG$_{M40}$ induced with doxycycline for 96 h cultured in presence or not of Rspo1 and treated or not with the proteosome inhibitor Bortezomib (5 μM, 6 and 12 h).E. Comet assay of mPrOs-ERG$_{M40}$ induced or not with doxycycline (96 h) and cultured in the presence or not of Rspo1. (n > 100 comets analyzed per condition). Wilcoxon test, * = p value < 0.05; *** = p-value <0.001.F. Immunoblot analysis of DSBs markers γH2ax, p-53bp1, and p-Atm in mPrOs-ERG$_{M40}$ induced or not with doxycycline for 96 h cultured in presence or not of Rspo1 and treated or not with the Gsk3β inhibitor CHIR99021 (5 μM, 6 days).

and commonly considered one of the earliest events in prostate tumor-igenesis [50,54–56]. Transcriptomic analysis of human PCa (cBioPortal, https://www.cbioportal.org) shows a slight, but significant, increase of *NKX3.1* expression in tumor compared to normal tissue, which posi-tively correlates with *ERG* expression in ERG positive PCa (Supple-mentary Figs. S6A–B). Immunohistochemical analyses for ERG and NKX3.1 expression in human HGPIN and PCa show heterogeneous amounts of NKX3.1 protein in both ERG positive and ERG negative prostate lesions, with cells characterized by very low levels of NKX3.1 protein expression (Supplementary Fig. S6C and Supplementary Table S7). Notably, induction of ERG expression in LNCaP and 22Rv1 human PCa cell lines enhances *NKX3.1* transcription (Supplementary Fig. S6D), but substantially lowers the amount of NKX3.1 protein (Supplementary Fig. S6E).

ERG promotes DNA double strand breaks in prostate cancer cells (Supplementary Fig. S6E) [57–59], whereas NKX3.1 is involved in DNA damage repair in prostate epithelium [60–64]. Thus, ERG expression concomitant with loss of NKX3.1 could pose a major threat to genomic stability since ERG-induced DNA damage in mPrOs accumulates in the absence of Nkx3.1 (Fig. 5E–F), still remaining sub-lethal (Supplemen-tary Fig. S7D).

Mechanistically, Rspo1 withdrawal in ERG + mPrOs leads to massive β-Catenin degradation likely dependent by a profuse activity of Gsk3β, as suggested by the administration of the Gsk3β inhibitor CHIR99021 (Supplementary Figs. S7A–D). *In silico* prediction studies define Ser-185 and Ser-195 residues of both human and mouse NKX3.1 proteins as putative targets of Gsk3β. Similar to β-Catenin, CHIR99021 adminis-tration completely rescues Nkx3.1 protein levels and, in turn, reduces the amount of DNA damages in ERG + mPrOs cultured without Rspo1 (Fig. 5F).

3.4. ERG-dependent paracrine signals influence Arginase 1 expression in M1 macrophages

Tumorigenesis is considered an unfavorable event. Nutrient unbal-ance, changes in the activity of specific cellular pathways, uncontrolled proliferation and dedifferentiation are all crucial stress factors that trigger immediate cell autonomous and non-cell autonomous responses. Besides activation of potent tumor suppressive cellular pathways, innate and adaptive immune systems are rapidly recruited in areas of tissue abnormalities with the primary intent to eradicate atypical cells. Mac-rophages are an essential component of the innate immune system, a major constituent of normal tissues, and key players in tissue repair and remodeling under both homeostatic and stress conditions. However, epidemiological and clinical studies have defined macrophage-promoted chronic inflammation as a critical risk factor in epithelial tissues tumorigenesis [65]. Analysis of the wild type mPrOs secretome pointed out a robust connection between extracellular signals secreted by prostate progenitors and the innate immune system. Several deregulated proteins in mPrOs-ERG$_{M40}$ supernatants are known to have specific roles in macrophage functions (Fig. 6A), and CD68$^+$ macro-phages were found to infiltrate ERG + HGPIN lesions in human prostates (Fig. 6B; Supplementary Fig. S8A). To investigate possible roles of ERG in promoting a pro-inflammatory tissue microenvironment, primary macrophages derived from femurs of wild type mice were treated with IFNγ and LPS to induce the M1 polarization (Supplementary Fig. S8B) and exposed to the supernatant of wild type and ERG$_{M40}$ mPrOs either treated or not with doxycycline (Fig. 6C). Forty-eight hours later, expression of the M1 markers *Il1b*, *Tnfα* and *iNos*, and M2 markers *Arg1* and *Chil3* was analyzed by RT-qPCR (Fig. 6D). Compared to the un-conditioned medium, all supernatants decrease the expression of *Il1b* and *Tnfα* in M1 macrophages, leave *iNos* induction unaffected, but promote *Arginase 1*, not *Chil3*, transcription (Fig. 6D), which lowers the production of nitric oxide (NO) in M1 macrophages by competing with iNos for arginine metabolism. Interestingly, *Arginase 1* induction is significantly weaker in M1 macrophages conditioned with the supernatants of ERG + mPrOs than in all other conditions (Fig. 6E), supporting the thesis of a possible non-cell-autonomous function of ERG dedicated to transform inflammatory macrophages in a source of sub-lethal oxidative stress.

4. Discussion

Being the most prevalent alteration in prostate cancer, ERG rear-rangement was heavily studied in the past years from many different groups. *ERG* genomic rearrangement and expression is considered a very early event in the history of PCa, being identified in a significant fraction of HGPIN prostate lesions [18–22]. However, *in vitro* and *in vivo* ex-periments show that ERG expression *per se* is not sufficient to induce full prostate cell transformation [7,16,23–25], while it has been robustly associated to increased migratory and invasive potential of immortal-ized and malignant prostate cells [9,17,23,26]. Therefore, expression of ERG in early prostate lesions is hardly justified by its involvement in PCa progression towards more advanced stages of the disease.

In *Pten/Trp53* double-null mouse model of PCa, ERG expression lowers tumor aggressiveness by decreasing proliferation and promoting luminal differentiation of cancer cells [66]. ERG expression in mouse prostate organoids promotes prostate progenitors commitment towards the luminal lineage (Fig. 7 and [67]). Importantly, expansion of the luminal compartment occurs with concomitant contraction of the basal layer in prostate organoids (Fig. 7), which resembles the histologic feature of the HGPIN lesions [7].

Thinking about the possible barriers that pre-malignant cells have to overcome to potentially develop a frank prostatic carcinoma, prolifer-ation in the absence of stimuli is a top priority [68]. A further important feature of ERG$_{M40}$ expressing mPrOs is their ability to grow in absence of EGF, a condition that is not permissive for the growth of mouse prostate organoids (Cambuli et al., *submitted*; Chua et al., 2014; Drost et al., 2016; Karthaus et al., 2014). This result suggests that ERG$_{M40}$ expression in normal prostate cells could uncouple them from the proliferative signals controlling tissue homeostasis, thus making ERG + HGPIN cells "*master of their own destiny*" [68]. Among the proteins differentially secreted by ERG$_{M40}$ expressing mPrOs, Macrophage stimulating 1/Hepatocyte growth factor-like (Mst1), Angiogenin (Ang), Growth differentiation factor 15/Prostate derived factor/Macrophage inhibitory cytokine 1 (Gdf15), and Vegfα are of particular interest in this scenario because they are over-expressed/secreted in human prostate cancer and responsible for activating pro-survival and pro-proliferation pathways in prostate cancer cells [69–73]. Future studies will help disentangling the possible contribution of those factors to sustain ERG + pre-malignant prostate cells under limited growth conditions.

On the other hand, the lower number of Ki67+ cells, which marks all phases of the cell cycle with the exclusion of G0, in presence of unaf-fected cell cycle might suggest a role of ERG in the transition of prolif-erating prostate cells to a more quiescent status. Although in 3D prostate organoids, as well as in HGPIN prostate lesions, ERG activity is not sufficient *per se* to induce cell motility, according to the "go-or-grow" hypothesis this finding potentially highlights new traits of the pro-migratory phenotype that ERG expression establishes in malignant prostate cells.

Besides ERG expression, loss of NKX3.1 is also a very common con-dition in human PCa, and one of the few molecular alterations func-tionally associated with the early stages of tumorigenesis [48,74–77]. During mouse prostate organogenesis, Wnt signaling released from the urogenital stroma stimulates *Nkx3.1* expression in all the epithelial cells of ductal buds [46]. Here, Nkx3.1 preserves luminal stem cells, promotes differentiation of the luminal compartment by controlling the rate at which proliferating luminal cells exit the cell cycle, and regulates ductal morphogenesis [47,78–80]. In addition to its crucial role in controlling the homeostasis of the luminal compartment of the prostate, NKX3.1 safeguards genome stability in prostate cells by promoting DNA damage repair [60,61,81] and protect mitochondria from the harmful effects of
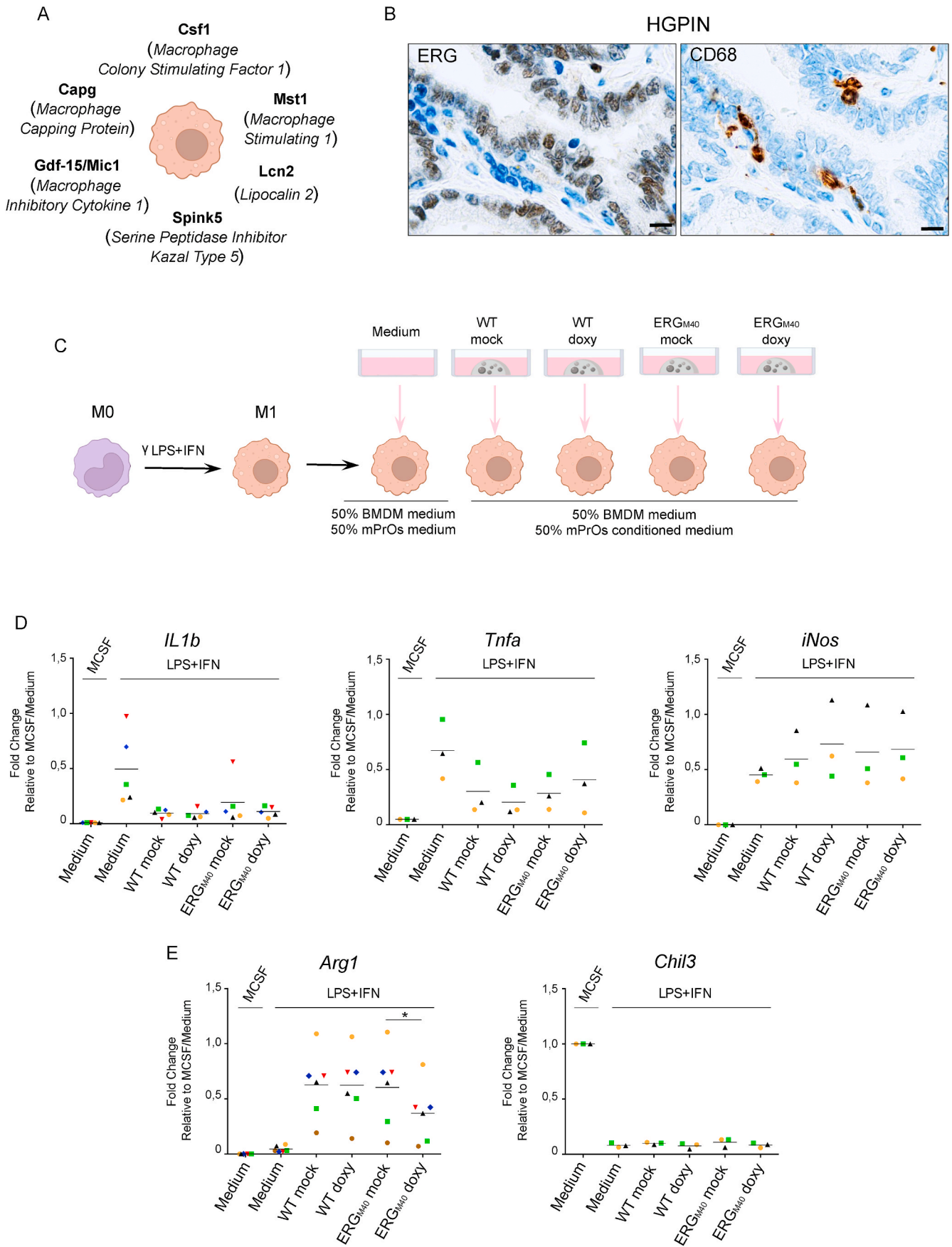
(caption on next page)

Fig. 6. *mPrOs extracellular signals modify the molecular profile of M1 macrophage*
A. Schematic representation of secreted proteins isolated in the screening with known functions in macrophages biology.B. Immunolocalization of CD68$^+$ macrophages in ERG + human high-grade prostatic intraepithelial neoplasia (HGPIN). Staining was performed on serial sections of paraffin embedded samples. Scale bar: 10 μm. C. Schematic representation of the experimental workflow. D-E. RT-qPCR analysis of genes characterizing M1 (*Il1b, Tnfα, iNos*; D) or M2 (*Arg1, Chil3*; E) polarized macrophages conditioned (1:1) with the supernatants of mPrOs-WT and mPrOs-ERG$_{M40}$ treated or not with doxycycline for 96 h. Unconditioned organoid medium was used as control. Statistical analyses were performed on at least n = 3 independent biological replicates. * = p value < 0.05; ** = p-value <0.01; *** = p-value <0.001.
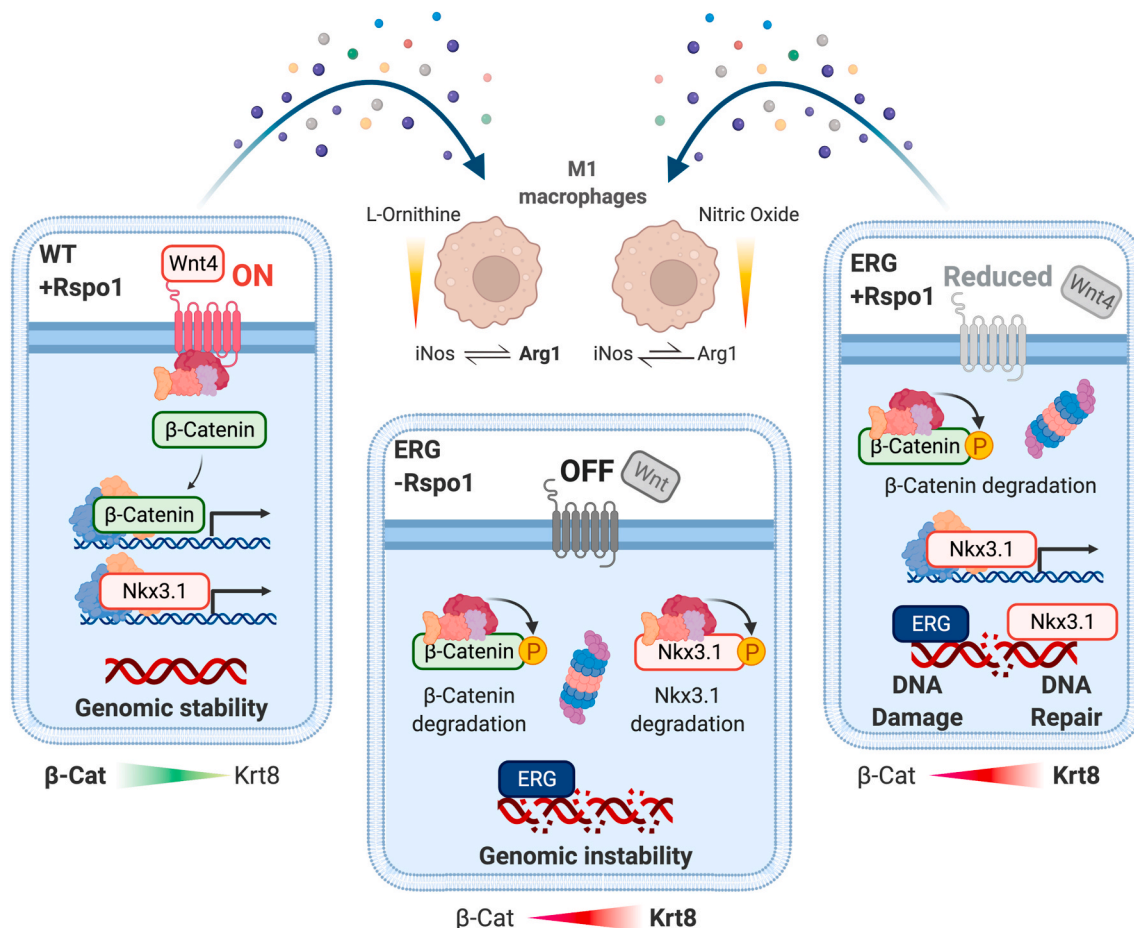
Fig. 7. Model of the molecular mechanisms primed by ERG to undermine cellular homeostasis and genome stability of adult prostate progenitors.

oxidative stress [63]. Heterozygous loss of *Nkx3.1* in adult mouse prostate generates hyperplastic and dysplastic pre-malignant epithelial lesions resembling human HGPIN [77,78,82]. Of note, F4/80+ macrophages are among the most abundant immune cells infiltrating the *Nkx3.1*-null mouse prostates, where they play a pivotal role in the development of HGPIN lesions by establishing a chronically inflamed oxidative microenvironment [83]. NKX3.1 expression is significantly reduced in almost 50% of HGPIN lesions [48,55,75]. Remarkably, NKX3.1 represses *ERG* transcription in prostate cells [84] and disfavors TMPRSS2-ERG genomic rearrangement [85], which supports the hypothesis that 8p21 deletions (NKX3.1) may precede 21q22 rearrangements (TMPRSS2-ERG fusion) in human prostate cancer harboring both molecular alterations [86]. However, ERG silences *NKX3.1* expression epigenetically [87] and promotes NKX3.1 protein degradation (Fig. 7), which implicates the possible reverse sequence of these two early events in prostate tumorigenesis. An important consequence of the coexistence of ERG expression and NKX3.1 loss in prostate cells is the substantial increase in DNA damage (Fig. 7). Recently, Hong and colleagues described a prominent role of ATR/CHK1 kinases - commonly activated by replication fork stalling - in promoting ERG proteolysis, while, in contrast, ATM/CHK2 signaling, triggered by DNA double strand breaks

(DSBs), does play no roles [88]. Likely, by favoring DSBs formation in prostate cells, ERG imposes a selective pressure on DSB repair pathways that might explain the frequent loss of DSBs repair effectors (*e.g.* P53, BRCA2, ATM) in ERG + human PCa [75].

Aberrant proliferation and genomic instability are pre-requisite for tumorigenesis, but it may be not sufficient in a complex environment such as a tissue. It is well-known that inflammation and immune activated cells play pivotal roles in the very early stage of the tumorigenic transformation [65]. Pre-cancerous cells need to influence and highjack immune response to "*avoid immune destruction*" [68]. Noteworthy, several proteins differentially secreted by ERG$_{M40}$ prostate organoids have been shown to influence the immune system, primarily macrophages. Pro-inflammatory macrophages release cytotoxic molecules and reactive oxygen species like nitrogen intermediates to trigger cell death. We have found that prostate organoids lessen the killing weaponry of M1 macrophages through secreted signals. This ability might be crucial *in vivo* to protect adult progenitor cells, and their regenerative potential, from the frequent inflammatory conditions affecting prostate gland, especially in aged men. Supernatants of ERG$_{M40}$ mPrOs still reduce the expression of cytotoxic molecules (*e.g.,* Tnfα and Il1β) in M1 macrophages, but *Arginase 1* expression is significantly less induced. This

condition should favor the production of nitric oxide (NO) from the catabolism of arginine through iNOS/Nos2 activity. Thus, by establishing a focal source of sub-lethal oxidative stress in the microenvironment, ERG could increase the rate of genetic and genomic alterations in prostate epithelial cells (Fig. 7).

To conclude, we speculate that by creating a sophisticated network of autocrine and paracrine extracellular signals in pre-cancerous human prostate lesions, ERG may orchestrate the prelude to malignant transformation.

Authors' contributions

Conception and design: M. Lorenzoni, D. De Felice, M. Gaspari, A. Alaimo, A. Lunardi.

Development of methodology: M. Lorenzoni, D. De Felice, F. Cambuli, M. Gaspari, A. Alaimo, A. Lunardi.

Acquisition of data: M. Lorenzoni, D. De Felice, A. Alaimo, S. Genovesi, G. Beccaceci, G. Di Donato, V. Foletto, F. Lorenzin, V. Weber, A. Savino, A. Cimadamore, R. Montironi, F.G. Carbone, M. Barbareschi, L. Avalle, A. Bertossi, A. Romanel, M.Gaspari.

Analysis and interpretation of data: M. Lorenzoni, D. De Felice, A. G. Beccaceci, G. Di Donato, V. Foletto, A. Savino, L. Avalle, A. Bertossi, F. Cambuli, F. Lorenzin, S. Genovesi, F.G. Carbone, M. Barbareschi, A. Cimadamore, R. Montironi, F. Demichelis, V. Poli, A. Romanel, G. Del Sal, M. Kruithof-de Julio, M. Gaspari, A. Alaimo, A. Lunardi.

Writing, review, and/or revision of the manuscript: M. Lorenzoni, D. De Felice, F. Demichelis, V. Poli, M. Kruithof-de Julio, G. Del Sal, M. Gaspari, A. Alaimo, A. Lunardi.

Administrative, technical, or material support: S. Genovesi, M. Lorenzoni, A. Cimadamore, D. De Felice, V. Foletto, V. Weber, A. Alaimo.

Study supervision: A. Lunardi.

Declaration of competing interest

The authors declare that they have no known competing financial interests or personal relationships that could have appeared to influence the work reported in this paper.

Acknowledgments

Appendix A. Supplementary data

Supplementary data to this article can be found online at https://doi.org/10.1016/j.canlet.2022.215612.

References

[1] J. Ferlay, I. Soerjomataram, R. Dikshit, S. Eser, C. Mathers, M. Rebelo, D.M. Parkin, D. Forman, F. Bray, Cancer incidence and mortality worldwide: sources, methods and major patterns in GLOBOCAN 2012, Int. J. Cancer 136 (2015) E359–E386, https://doi.org/10.1002/ijc.29210.

[2] G. Attard, C. Parker, R.A. Eeles, F. Schröder, S.A. Tomlins, I. Tannock, C.G. Drake, J.S. de Bono, Prostate cancer, Lancet 387 (2016) 70–82, https://doi.org/10.1016/S0140-6736(14)61947-4.

[3] R. Hodson, Prostate cancer: 4 big questions, Nature 528 (2015) S137, https://doi.org/10.1038/528S137a.

[4] T. Nyberg, D. Frost, D. Barrowdale, D.G. Evans, E. Bancroft, J. Adlard, M. Ahmed, J. Barwell, A.F. Brady, C. Brewer, J. Cook, R. Davidson, A. Donaldson, J. Eason, H. Gregory, A. Henderson, L. Izatt, M.J. Kennedy, C. Miller, P.J. Morrison, A. Murray, K.-R. Ong, M. Porteous, C. Pottinger, M.T. Rogers, L. Side, K. Snape, L. Walker, M. Tischkowitz, R. Eeles, D.F. Easton, A.C. Antoniou, Prostate cancer risks for male BRCA1 and BRCA2 mutation carriers: a prospective cohort study, Eur. Urol. 77 (2020) 24–35, https://doi.org/10.1016/j.eururo.2019.08.025.

[5] M.M. Shen, C. Abate-Shen, Molecular genetics of prostate cancer: new prospects for old challenges, Genes Dev. 24 (2010) 1967–2000, https://doi.org/10.1101/gad.1965810.

[6] D.G. Bostwick, J. Qian, High-grade prostatic intraepithelial neoplasia, Mod. Pathol. 17 (2004) 360–379, https://doi.org/10.1038/modpathol.3800053.

[7] O. Klezovitch, M. Risk, I. Coleman, J.M. Lucas, M. Null, L.D. True, P.S. Nelson, V. Vasioukhin, A causal role for ERG in neoplastic transformation of prostate epithelium, Proc. Natl. Acad. Sci. U. S. A. 105 (2008) 2105–2110, https://doi.org/10.1073/pnas.0711711105.

[8] R. Montironi, R. Mazzucchelli, A. Lopez-Beltran, L. Cheng, M. Scarpelli, Mechanisms of disease: high-grade prostatic intraepithelial neoplasia and other proposed preneoplastic lesions in the prostate, Nat. Clin. Pract. Urol. 4 (2007) 321–332, https://doi.org/10.1038/ncpuro0815.

[9] F. Demichelis, M.A. Rubin, TMPRSS2-ETS fusion prostate cancer: biological and clinical implications, J. Clin. Pathol. 60 (2007) 1185–1186, https://doi.org/10.1136/jcp.2007.046557.

[10] C. Kumar-Sinha, S.A. Tomlins, A.M. Chinnaiyan, Recurrent gene fusions in prostate cancer, Nat. Rev. Cancer 8 (2008) 497–511, https://doi.org/10.1038/nrc2402.

[11] J. Yu, J. Yu, R.-S. Mani, Q. Cao, C.J. Brenner, X. Cao, X. Wang, L. Wu, J. Li, M. Hu, Y. Gong, H. Cheng, B. Laxman, A. Vellaichamy, S. Shankar, Y. Li, S. M. Dhanasekaran, R. Morey, T. Barrette, R.J. Lonigro, S.A. Tomlins, S. Varambally, Z.S. Qin, A.M. Chinnaiyan, An integrated network of androgen receptor, polycomb, and TMPRSS2-ERG gene fusions in prostate cancer progression, Cancer Cell 17 (2010) 443–454, https://doi.org/10.1016/j.ccr.2010.03.018.

[12] S.A. Lacadie, L.I. Zon, The ERGonomics of hematopoietic stem cell self-renewal, Genes Dev. 25 (2011) 289–293, https://doi.org/10.1101/gad.2031511.

[13] S.J. Loughran, E.A. Kruse, D.F. Hacking, C.A. de Graaf, C.D. Hyland, T.A. Willson, K.J. Henley, S. Ellis, A.K. Voss, D. Metcalf, D.J. Hilton, W.S. Alexander, B.T. Kile, The transcription factor Erg is essential for definitive hematopoiesis and the function of adult hematopoietic stem cells, Nat. Immunol. 9 (2008) 810–819, https://doi.org/10.1038/ni.1617.

[14] S.A. Tomlins, D.R. Rhodes, S. Perner, S.M. Dhanasekaran, R. Mehra, X.-W. Sun, S. Varambally, X. Cao, J. Tchinda, R. Kuefer, C. Lee, J.E. Montie, R.B. Shah, K. J. Pienta, M.A. Rubin, A.M. Chinnaiyan, Recurrent fusion of TMPRSS2 and ETS transcription factor genes in prostate cancer, Science 310 (2005) 644–648, https://doi.org/10.1126/science.1117679.

[15] F. Demichelis, K. Fall, S. Perner, O. Andrén, F. Schmidt, S.R. Setlur, Y. Hoshida, J.-M. Mosquera, Y. Pawitan, C. Lee, H.-O. Adami, L.A. Mucci, P.W. Kantoff, S.-O. Andersson, A.M. Chinnaiyan, J.-E. Johansson, M.A. Rubin, TMPRSS2:ERG gene fusion associated with lethal prostate cancer in a watchful waiting cohort, Oncogene 26 (2007) 4596–4599, https://doi.org/10.1038/sj.onc.1210237.

[16] J.C. King, J. Xu, J. Wongvipat, H. Hieronymus, B.S. Carver, D.H. Leung, B. S. Taylor, C. Sander, R.D. Cardiff, S.S. Couto, W.L. Gerald, C.L. Sawyers, Cooperativity of TMPRSS2-ERG with PI3-kinase pathway activation in prostate oncogenesis, Nat. Genet. 41 (2009) 524–526, https://doi.org/10.1038/ng.371.

[17] S. Perner, F.H. Schmidt, M.D. Hofer, R. Kuefer, M. Rubin, [TMPRSS2-ETS gene fusion in prostate cancer], Urologe 46 (2007) 754–760, https://doi.org/10.1007/s00120-007-1347-0.

[18] H. He, A.O. Osunkoya, P. Carver, S. Falzarano, E. Klein, C. Magi-Galluzzi, M. Zhou, Expression of ERG protein, a prostate cancer specific marker, in high grade prostatic intraepithelial neoplasia (HGPIN): lack of utility to stratify cancer risks

associated with HGPIN, BJU Int. 110 (2012) E751–E755, https://doi.org/10.1111/j.1464-410X.2012.11557.x.

[19] S.L. Lee, D. Yu, C. Wang, R. Saba, S. Liu, K. Trpkov, B. Donnelly, T.A. Bismar, ERG expression in prostate needle biopsy: potential diagnostic and prognostic implications, Appl. Immunohistochem. Mol. Morphol. 23 (2015) 499–505, https://doi.org/10.1097/PAI.0000000000000119.

[20] C.L. Morais, L.B. Guedes, J. Hicks, A.S. Baras, A.M. De Marzo, T.L. Lotan, ERG and PTEN status of isolated high-grade PIN occurring in cystoprostatectomy specimens without invasive prostatic adenocarcinoma, Hum. Pathol. 55 (2016) 117–125, https://doi.org/10.1016/j.humpath.2016.04.017.

[21] J.-M. Mosquera, S. Perner, E.M. Genega, M. Sanda, M.D. Hofer, K.D. Mertz, P. L. Paris, J. Simko, T.A. Bismar, G. Ayala, R.B. Shah, M. Loda, M.A. Rubin, Characterization of TMPRSS2-ERG fusion high-grade prostatic intraepithelial neoplasia and potential clinical implications, Clin. Cancer Res. 14 (2008) 3380–3385, https://doi.org/10.1158/1078-0432.CCR-07-5194.

[22] L.H. Teng, C. Wang, M. Dolph, B. Donnelly, T.A. Bismar, ERG protein expression is of limited prognostic value in men with localized prostate cancer, ISRN Urol. (2013), 786545, https://doi.org/10.1155/2013/786545, 2013.

[23] B.S. Carver, J. Tran, A. Gopalan, Z. Chen, S. Shaikh, A. Carracedo, A. Alimonti, C. Nardella, S. Varmeh, P.T. Scardino, C. Cordon-Cardo, W. Gerald, P.P. Pandolfi, Aberrant ERG expression cooperates with loss of PTEN to promote cancer progression in the prostate, Nat. Genet. 41 (2009) 619–624, https://doi.org/10.1038/ng.370.

[24] Y. Chen, P. Chi, S. Rockowitz, P.J. Iaquinta, T. Shamu, S. Shukla, D. Gao, I. Sirota, B.S. Carver, J. Wongvipat, H.I. Scher, D. Zheng, C.L. Sawyers, ETS factors reprogram the androgen receptor cistrome and prime prostate tumorigenesis in response to PTEN loss, Nat. Med. 19 (2013) 1023–1029, https://doi.org/10.1038/nm.3216.

[25] S.A. Tomlins, B. Laxman, S. Varambally, X. Cao, J. Yu, B.E. Helgeson, Q. Cao, J. R. Prensner, M.A. Rubin, R.B. Shah, R. Mehra, A.M. Chinnaiyan, Role of the TMPRSS2-ERG gene fusion in prostate cancer, Neoplasia 10 (2008) 177–188, https://doi.org/10.1593/neo.07822.

[26] A. Alaimo, M. Lorenzoni, P. Ambrosino, A. Bertossi, A. Bisio, A. Macchia, E. Zoni, S. Genovesi, F. Cambuli, V. Foletto, D. De Felice, M.V. Soldovieri, I. Mosca, F. Gandolfi, M. Brunelli, G. Petris, A. Cereseto, A. Villarroel, G. Thalmann, F. G. Carbone, M. Kruithof-de Julio, M. Barbareschi, A. Romanel, M. Taglialatela, A. Lunardi, Calcium cytotoxicity sensitizes prostate cancer cells to standard-of-care treatments for locally advanced tumors, Cell Death Dis. 11 (2020) 1039, https://doi.org/10.1038/s41419-020-03256-5.

[27] F. Cambuli, V. Foletto, A. Alaimo, D. De Felice, F. Gandolfi, M.D. Palumbieri, M. Zaffagni, S. Genovesi, M. Lorenzoni, M. Celotti, E. Bertossio, G. Mazzero, A. Bertossi, A. Bisio, F. Berardinelli, A. Antoccia, M. Gaspari, M. Barbareschi, M. Fiorentino, M.M. Shen, M. Loda, A. Romanel, A. Lunardi, Intra-epithelial non-canonical Activin A signalling safeguards prostate progenitor quiescence, Cancer Biol. (2021), https://doi.org/10.1101/2021.03.05.433921.

[28] J. Drost, W.R. Karthaus, D. Gao, E. Driehuis, C.L. Sawyers, Y. Chen, H. Clevers, Organoid culture systems for prostate epithelial and cancer tissue, Nat. Protoc. 11 (2016) 347–358, https://doi.org/10.1038/nprot.2016.006.

[29] W.R. Karthaus, P.J. Iaquinta, J. Drost, A. Gracanin, R. van Boxtel, J. Wongvipat, C. M. Dowling, D. Gao, H. Begthel, N. Sachs, R.G.J. Vries, E. Cuppen, Y. Chen, C. L. Sawyers, H.C. Clevers, Identification of multipotent luminal progenitor cells in human prostate organoid cultures, Cell 159 (2014) 163–175, https://doi.org/10.1016/j.cell.2014.08.017.

[30] M. Pizzato, O. Erlwein, D. Bonsall, S. Kaye, D. Muir, M.O. McClure, A one-step SYBR Green I-based product-enhanced reverse transcriptase assay for the quantitation of retroviruses in cell culture supernatants, J. Virol. Methods 156 (2009) 1–7, https://doi.org/10.1016/j.jviromet.2008.10.012.

[31] K. Eichelbaum, J. Krijgsveld, Combining pulsed SILAC labeling and click-chemistry for quantitative secretome analysis, Methods Mol. Biol. 1174 (2014) 101–114, https://doi.org/10.1007/978-1-4939-0944-5_7.

[32] K. Eichelbaum, M. Winter, M. Berriel Diaz, S. Herzig, J. Krijgsveld, Selective enrichment of newly synthesized proteins for quantitative secretome analysis, Nat. Biotechnol. 30 (2012) 984–990, https://doi.org/10.1038/nbt.2356.

[33] J. Rappsilber, M. Mann, Y. Ishihama, Protocol for micro-purification, enrichment, pre-fractionation and storage of peptides for proteomics using StageTips, Nat. Protoc. 2 (2007) 1896–1906, https://doi.org/10.1038/nprot.2007.261.

[34] S. Tyanova, T. Temu, P. Sinitcyn, A. Carlson, M.Y. Hein, T. Geiger, M. Mann, J. Cox, The Perseus computational platform for comprehensive analysis of (prote) omics data, Nat. Methods 13 (2016) 731–740, https://doi.org/10.1038/nmeth.3901.

[35] J. Cox, M.Y. Hein, C.A. Luber, I. Paron, N. Nagaraj, M. Mann, Accurate proteome-wide label-free quantification by delayed normalization and maximal peptide ratio extraction, termed MaxLFQ, Mol. Cell. Proteomics 13 (2014) 2513–2526, https://doi.org/10.1074/mcp.M113.031591.

[36] C. von Mering, M. Huynen, D. Jaeggi, S. Schmidt, P. Bork, B. Snel, STRING: a database of predicted functional associations between proteins, Nucleic Acids Res. 31 (2003) 258–261, https://doi.org/10.1093/nar/gkg034.

[37] D. Szklarczyk, A.L. Gable, D. Lyon, A. Junge, S. Wyder, J. Huerta-Cepas, M. Simonovic, N.T. Doncheva, J.H. Morris, P. Bork, L.J. Jensen, C. von Mering, STRING v11: protein-protein association networks with increased coverage, supporting functional discovery in genome-wide experimental datasets, Nucleic Acids Res. 47 (2019) D607–D613, https://doi.org/10.1093/nar/gky1131.

[38] C.W. Chua, M. Shibata, M. Lei, R. Toivanen, L.J. Barlow, S.K. Bergren, K.K. Badani, J.M. McKiernan, M.C. Benson, H. Hibshoosh, M.M. Shen, Single luminal epithelial progenitors can generate prostate organoids in culture, Nat. Cell Biol. 16 (2014) 951–961, https://doi.org/10.1038/ncb3047, 1–4.

[39] D. Gao, I. Vela, A. Sboner, P.J. Iaquinta, W.R. Karthaus, A. Gopalan, C. Dowling, J. N. Wanjala, E.A. Undvall, V.K. Arora, J. Wongvipat, M. Kossai, S. Ramazanoglu, L. P. Barboza, W. Di, Z. Cao, Q.F. Zhang, I. Sirota, L. Ran, T.Y. MacDonald, H. Beltran, J.-M. Mosquera, K.A. Touijer, P.T. Scardino, V.P. Laudone, K.R. Curtis, D. E. Rathkopf, M.J. Morris, D.C. Danila, S.F. Slovin, S.B. Solomon, J.A. Eastham, P. Chi, B. Carver, M.A. Rubin, H.I. Scher, H. Clevers, C.L. Sawyers, Y. Chen, Organoid cultures derived from patients with advanced prostate cancer, Cell 159 (2014) 176–187, https://doi.org/10.1016/j.cell.2014.08.016.

[40] A. Nurdin, Y. Hoshi, T. Yoneyama, E. Miyauchi, M. Tachikawa, M. Watanabe, T. Terasaki, Global and targeted proteomics of prostate cancer cell secretome: combination of 2-dimensional image-converted analysis of liquid chromatography and mass spectrometry and in silico selection selected reaction monitoring analysis, J. Pharmaceut. Sci. 105 (2016) 3440–3452, https://doi.org/10.1016/j.xphs.2016.08.013.

[41] M.P. Pavlou, E.P. Diamandis, The cancer cell secretome: a good source for discovering biomarkers? J. Proteomics 73 (2010) 1896–1906, https://doi.org/10.1016/j.jprot.2010.04.003.

[42] S. Principe, Y. Kim, S. Fontana, V. Ignatchenko, J.O. Nyalwidhe, R.S. Lance, D. A. Troyer, R. Alessandro, O.J. Semmes, T. Kislinger, R.R. Drake, J.A. Medin, Identification of prostate-enriched proteins by in-depth proteomic analyses of expressed prostatic secretions in urine, J. Proteome Res. 11 (2012) 2386–2396, https://doi.org/10.1021/pr2011236.

[43] D.W. Huang, B.T. Sherman, R. Stephens, M.W. Baseler, H.C. Lane, R.A. Lempicki, DAVID gene ID conversion tool, Bioinformation 2 (2008) 428–430, https://doi.org/10.6026/97320630002428.

[44] D.W. Huang, B.T. Sherman, R.A. Lempicki, Bioinformatics enrichment tools: paths toward the comprehensive functional analysis of large gene lists, Nucleic Acids Res. 37 (2009) 1–13, https://doi.org/10.1093/nar/gkn923.

[45] A.-A. Chassot, S.T. Bradford, A. Auguste, E.P. Gregoire, E. Pailhoux, D.G. de Rooij, A. Schedl, M.-C. Chaboissier, WNT4 and RSPO1 together are required for cell proliferation in the early mouse gonad, Development 139 (2012) 4461–4472, https://doi.org/10.1242/dev.078972.

[46] M. Kruithof-de Julio, M. Shibata, N. Desai, M. Reynon, M.V. Halili, Y.-P. Hu, S. M. Price, C. Abate-Shen, M.M. Shen, Canonical Wnt signaling regulates Nkx3.1 expression and luminal epithelial differentiation during prostate organogenesis, Dev. Dynam. 242 (2013) 1160–1171, https://doi.org/10.1002/dvdy.24008.

[47] X. Wang, M. Kruithof-de Julio, K.D. Economides, D. Walker, H. Yu, M.V. Halili, Y.-P. Hu, S.M. Price, C. Abate-Shen, M.M. Shen, A luminal epithelial stem cell that is a cell of origin for prostate cancer, Nature 461 (2009) 495–500, https://doi.org/10.1038/nature08361.

[48] S.C. Baca, D. Prandi, M.S. Lawrence, J.M. Mosquera, A. Romanel, Y. Drier, K. Park, N. Kitabayashi, T.Y. MacDonald, M. Ghandi, E. Van Allen, G.V. Kryukov, A. Sboner, J.-P. Theurillat, T.D. Soong, E. Nickerson, D. Auclair, A. Tewari, H. Beltran, R. C. Onofrio, G. Boysen, C. Guiducci, C.E. Barbieri, K. Cibulskis, A. Sivachenko, S. L. Carter, G. Saksena, D. Voet, A.H. Ramos, W. Winckler, M. Cipicchio, K. Ardlie, P. W. Kantoff, M.F. Berger, S.B. Gabriel, T.R. Golub, M. Meyerson, E.S. Lander, O. Elemento, G. Getz, F. Demichelis, M.A. Rubin, L.A. Garraway, Punctuated evolution of prostate cancer genomes, Cell 153 (2013) 666–677, https://doi.org/10.1016/j.cell.2013.03.021.

[49] C.R. Bethel, D. Faith, X. Li, B. Guan, J.L. Hicks, F. Lan, R.B. Jenkins, C.J. Bieberich, A.M. De Marzo, Decreased NKX3.1 protein expression in focal prostatic atrophy, prostatic intraepithelial neoplasia, and adenocarcinoma: association with gleason score and chromosome 8p deletion, Cancer Res. 66 (2006) 10683–10690, https://doi.org/10.1158/0008-5472.CAN-06-0963.

[50] M.J. Kim, R.D. Cardiff, N. Desai, W.A. Banach-Petrosky, R. Parsons, M.M. Shen, C. Abate-Shen, Cooperativity of Nkx3.1 and Pten loss of function in a mouse model of prostate carcinogenesis, Proc. Natl. Acad. Sci. U. S. A. 99 (2002) 2884–2889, https://doi.org/10.1073/pnas.042688999.

[51] M.C. Markowski, C. Bowen, E.P. Gelmann, Inflammatory cytokines induce phosphorylation and ubiquitination of prostate suppressor protein NKX3.1, Cancer Res. 68 (2008) 6896–6901, https://doi.org/10.1158/0008-5472.CAN-08-0578.

[52] B.S. Taylor, N. Schultz, H. Hieronymus, A. Gopalan, Y. Xiao, B.S. Carver, V. K. Arora, P. Kaushik, E. Cerami, B. Reva, Y. Antipin, N. Mitsiades, T. Landers, I. Dolgalev, J.E. Major, M. Wilson, N.D. Socci, A.E. Lash, A. Heguy, J.A. Eastham, H.I. Scher, V.E. Reuter, P.T. Scardino, C. Sander, C.L. Sawyers, W.L. Gerald, Integrative genomic profiling of human prostate cancer, Cancer Cell 18 (2010) 11–22, https://doi.org/10.1016/j.ccr.2010.05.026.

[53] A. Padmanabhan, V. Rao, A.M. De Marzo, C.J. Bieberich, Regulating NKX3.1 stability and function: post-translational modifications and structural determinants, Prostate 76 (2016) 523–533, https://doi.org/10.1002/pros.23144.

[54] E. Asatiani, W.-X. Huang, A. Wang, E. Rodriguez Ortner, L.R. Cavalli, B.R. Haddad, E.P. Gelmann, Deletion, methylation, and expression of the NKX3.1 suppressor gene in primary human prostate cancer, Cancer Res. 65 (2005) 1164–1173, https://doi.org/10.1158/0008-5472.CAN-04-2688.

[55] C. Bowen, L. Bubendorf, H.J. Voeller, R. Slack, N. Willi, G. Sauter, T.C. Gasser, P. Koivisto, E.E. Lack, J. Kononen, O.P. Kallioniemi, E.P. Gelmann, Loss of NKX3.1 expression in human prostate cancers correlates with tumor progression, Cancer Res. 60 (2000) 6111–6115.

[56] B. Gurel, T.Z. Ali, E.A. Montgomery, S. Begum, J. Hicks, M. Goggins, C.G. Eberhart, D.P. Clark, C.J. Bieberich, J.I. Epstein, A.M. De Marzo, NKX3.1 as a marker of prostatic origin in metastatic tumors, Am. J. Surg. Pathol. 34 (2010) 1097–1105, https://doi.org/10.1097/PAS.0b013e3181e6cbf3.

[57] J.C. Brenner, B. Ateeq, Y. Li, A.K. Yocum, Q. Cao, I.A. Asangani, S. Patel, X. Wang, H. Liang, J. Yu, N. Palanisamy, J. Siddiqui, W. Yan, X. Cao, R. Mehra, A. Sabolch, V. Basrur, R.J. Lonigro, J. Yang, S.A. Tomlins, C.A. Maher, K.S.J. Elenitoba-Johnson, M. Hussain, N.M. Navone, K.J. Pienta, S. Varambally, F.Y. Feng, A.

M. Chinnaiyan, Mechanistic rationale for inhibition of poly(ADP-ribose) polymerase in ETS gene fusion-positive prostate cancer, Cancer Cell 19 (2011) 664–678, https://doi.org/10.1016/j.ccr.2011.04.010.

[58] P. Chatterjee, G.S. Choudhary, A. Sharma, K. Singh, W.D. Heston, J. Ciezki, E. A. Klein, A. Almasan, PARP inhibition sensitizes to low dose-rate radiation TMPRSS2-ERG fusion gene-expressing and PTEN-deficient prostate cancer cells, PLoS One 8 (2013), e60408, https://doi.org/10.1371/journal.pone.0060408.

[59] P. Chatterjee, G.S. Choudhary, T. Alswillah, X. Xiong, W.D. Heston, C. Magi-Galluzzi, J. Zhang, E.A. Klein, A. Almasan, The TMPRSS2-ERG gene fusion blocks XRCC4-mediated nonhomologous end-joining repair and radiosensitizes prostate cancer cells to PARP inhibition, Mol. Cancer Therapeut. 14 (2015) 1896–1906, https://doi.org/10.1158/1535-7163.MCT-14-0865.

[60] C. Bowen, E.P. Gelmann, NKX3.1 activates cellular response to DNA damage, Cancer Res. 70 (2010) 3089–3097, https://doi.org/10.1158/0008-5472.CAN-09-3138.

[61] C. Bowen, J.-H. Ju, J.-H. Lee, T.T. Paull, E.P. Gelmann, Functional activation of ATM by the prostate cancer suppressor NKX3.1, Cell Rep. 4 (2013) 516–529, https://doi.org/10.1016/j.celrep.2013.06.039.

[62] X. Ouyang, T.L. DeWeese, W.G. Nelson, C. Abate-Shen, Loss-of-function of Nkx3.1 promotes increased oxidative damage in prostate carcinogenesis, Cancer Res. 65 (2005) 6773–6779, https://doi.org/10.1158/0008-5472.CAN-05-1948.

[63] A. Papachristodoulou, A. Rodriguez-Calero, S. Panja, E. Margolskee, R.K. Virk, T. A. Milner, L.P. Martina, J.Y. Kim, M. Di Bernardo, A.B. Williams, E.A. Maliza, J. M. Caputo, C. Haas, V. Wang, G.J. De Castro, S. Wenske, H. Hibshoosh, J. M. McKiernan, M.M. Shen, M.A. Rubin, A. Mitrofanova, A. Dutta, C. Abate-Shen, NKX3.1 localization to mitochondria suppresses prostate cancer initiation, Cancer Discov. 11 (2021) 2316–2333, https://doi.org/10.1158/2159-8290.CD-20-1765.

[64] H. Zhang, T. Zheng, C.W. Chua, M. Shen, E.P. Gelmann, Nkx3.1 controls the DNA repair response in the mouse prostate, Prostate 76 (2016) 402–408, https://doi.org/10.1002/pros.23131.

[65] E. Elinav, R. Nowarski, C.A. Thaiss, B. Hu, C. Jin, R.A. Flavell, Inflammation-induced cancer: crosstalk between tumours, immune cells and microorganisms, Nat. Rev. Cancer 13 (2013) 759–771, https://doi.org/10.1038/nrc3611.

[66] A.M. Blee, Y. He, Y. Yang, Z. Ye, Y. Yan, Y. Pan, T. Ma, J. Dugdale, E. Kuehn, M. Kohli, R. Jimenez, Y. Chen, W. Xu, L. Wang, H. Huang, TMPRSS2-ERG controls luminal epithelial lineage and antiandrogen sensitivity in PTEN and TP53-mutated prostate cancer, Clin. Cancer Res. 24 (2018) 4551–4565, https://doi.org/10.1158/1078-0432.CCR-18-0653.

[67] F. Li, Q. Yuan, W. Di, X. Xia, Z. Liu, N. Mao, L. Li, C. Li, J. He, Y. Li, W. Guo, X. Zhang, Y. Zhu, R. Aji, S. Wang, X. Tong, H. Ji, P. Chi, B. Carver, Y. Wang, Y. Chen, D. Gao, ERG orchestrates chromatin interactions to drive prostate cell fate reprogramming, J. Clin. Invest. 130 (2020) 5924–5941, https://doi.org/10.1172/JCI137967.

[68] D. Hanahan, R.A. Weinberg, Hallmarks of cancer: the next generation, Cell 144 (2011) 646–674, https://doi.org/10.1016/j.cell.2011.02.013.

[69] K. Ganapathy, S. Staklinski, M.F. Hasan, R. Ottman, T. Andl, A.E. Berglund, J. Y. Park, R. Chakrabarti, Multifaceted function of MicroRNA-299-3p fosters an antitumor environment through modulation of androgen receptor and VEGFA signaling pathways in prostate cancer, Sci. Rep. 10 (2020) 5167, https://doi.org/10.1038/s41598-020-62038-3.

[70] S. Ibaragi, N. Yoshioka, S. Li, M.G. Hu, S. Hirukawa, P.M. Sadow, G.-F. Hu, Neamine inhibits prostate cancer growth by suppressing angiogenin-mediated rRNA transcription, Clin. Cancer Res. 15 (2009) 1981–1988, https://doi.org/10.1158/1078-0432.CCR-08-2593.

[71] S. Soker, M. Kaefer, M. Johnson, M. Klagsbrun, A. Atala, M.R. Freeman, Vascular endothelial growth factor-mediated autocrine stimulation of prostate tumor cells coincides with progression to a malignant phenotype, Am. J. Pathol. 159 (2001) 651–659, https://doi.org/10.1016/S0002-9440(10)61736-1.

[72] W. Wang, X. Yang, J. Dai, Y. Lu, J. Zhang, E.T. Keller, Prostate cancer promotes a vicious cycle of bone metastasis progression through inducing osteocytes to secrete GDF15 that stimulates prostate cancer growth and invasion, Oncogene 38 (2019) 4540–4559, https://doi.org/10.1038/s41388-019-0736-3.

[73] H.-P. Yao, Y.-Q. Zhou, R. Zhang, M.-H. Wang, MSP-RON signalling in cancer: pathogenesis and therapeutic potential, Nat. Rev. Cancer 13 (2013) 466–481, https://doi.org/10.1038/nrc3545.

[74] C. Abate-Shen, M.M. Shen, E. Gelmann, Integrating differentiation and cancer: the Nkx3.1 homeobox gene in prostate organogenesis and carcinogenesis, Differentiation 76 (2008) 717–727, https://doi.org/10.1111/j.1432-0436.2008.00292.x.

[75] Cancer Genome Atlas Research Network, The molecular taxonomy of primary prostate cancer, Cell 163 (2015) 1011–1025, https://doi.org/10.1016/j.cell.2015.10.025.

[76] S.M.G. Espiritu, L.Y. Liu, Y. Rubanova, V. Bhandari, E.M. Holgersen, L.M. Szyca, N. S. Fox, M.L.K. Chua, T.N. Yamaguchi, L.E. Heisler, J. Livingstone, J. Wintersinger, F. Yousif, E. Lalonde, A. Rouette, A. Salcedo, K.E. Houlahan, C.H. Li, V. Huang, M. Fraser, T. van der Kwast, Q.D. Morris, R.G. Bristow, P.C. Boutros, The evolutionary landscape of localized prostate cancers drives clinical aggression, Cell 173 (2018) 1003–1013, https://doi.org/10.1016/j.cell.2018.03.029, e15.

[77] M.J. Kim, R. Bhatia-Gaur, W.A. Banach-Petrosky, N. Desai, Y. Wang, S. W. Hayward, G.R. Cunha, R.D. Cardiff, M.M. Shen, C. Abate-Shen, Nkx3.1 mutant mice recapitulate early stages of prostate carcinogenesis, Cancer Res. 62 (2002) 2999–3004.

[78] R. Bhatia-Gaur, A.A. Donjacour, P.J. Sciavolino, M. Kim, N. Desai, P. Young, C. R. Norton, T. Gridley, R.D. Cardiff, G.R. Cunha, C. Abate-Shen, M.M. Shen, Roles for Nkx3.1 in prostate development and cancer, Genes Dev. 13 (1999) 966–977, https://doi.org/10.1101/gad.13.8.966.

[79] J.A. Magee, S.A. Abdulkadir, J. Milbrandt, Haploinsufficiency at the Nkx3.1 locus. A paradigm for stochastic, dosage-sensitive gene regulation during tumor initiation, Cancer Cell 3 (2003) 273–283, https://doi.org/10.1016/s1535-6108(03)00047-3.

[80] F. Talos, A. Mitrofanova, S.K. Bergren, A. Califano, M.M. Shen, A computational systems approach identifies synergistic specification genes that facilitate lineage conversion to prostate tissue, Nat. Commun. 8 (2017), 14662, https://doi.org/10.1038/ncomms14662.

[81] C.-C. Yang, A. Chung, C.-Y. Ku, L.M. Brill, R. Williams, D.A. Wolf, Systems analysis of the prostate tumor suppressor NKX3.1 supports roles in DNA repair and luminal cell differentiation, F1000 Res. 3 (2014) 115, https://doi.org/10.12688/f1000research.3818.2.

[82] S. Irshad, C. Abate-Shen, Modeling prostate cancer in mice: something old, something new, something premalignant, something metastatic, Cancer Metastasis Rev. 32 (2013) 109–122, https://doi.org/10.1007/s10555-012-9409-1.

[83] C. Le Magnen, R.K. Virk, A. Dutta, J.Y. Kim, S. Panja, Z.A. Lopez-Bujanda, A. Califano, C.G. Drake, A. Mitrofanova, C. Abate-Shen, Cooperation of loss of NKX3.1 and inflammation in prostate cancer initiation, Dis. Model Mech. 11 (2018), dmm035139, https://doi.org/10.1242/dmm.035139.

[84] R. Thangapazham, F. Saenz, S. Katta, A.A. Mohamed, S.-H. Tan, G. Petrovics, S. Srivastava, A. Dobi, Loss of the NKX3.1 tumorsuppressor promotes the TMPRSS2-ERG fusion gene expression in prostate cancer, BMC Cancer 14 (2014) 16, https://doi.org/10.1186/1471-2407-14-16.

[85] C. Bowen, T. Zheng, E.P. Gelmann, NKX3.1 suppresses TMPRSS2-ERG gene rearrangement and mediates repair of androgen receptor-induced DNA damage, Cancer Res. 75 (2015) 2686–2698, https://doi.org/10.1158/0008-5472.CAN-14-3387.

[86] J. Lapointe, C. Li, C.P. Giacomini, K. Salari, S. Huang, P. Wang, M. Ferrari, T. Hernandez-Boussard, J.D. Brooks, J.R. Pollack, Genomic profiling reveals alternative genetic pathways of prostate tumorigenesis, Cancer Res. 67 (2007) 8504–8510, https://doi.org/10.1158/0008-5472.CAN-07-0673.

[87] P. Kunderfranco, M. Mello-Grand, R. Cangemi, S. Pellini, A. Mensah, V. Albertini, A. Malek, G. Chiorino, C.V. Catapano, G.M. Carbone, ETS transcription factors control transcription of EZH2 and epigenetic silencing of the tumor suppressor gene Nkx3.1 in prostate cancer, PLoS One 5 (2010), e10547, https://doi.org/10.1371/journal.pone.0010547.

[88] Z. Hong, W. Zhang, D. Ding, Z. Huang, Y. Yan, W. Cao, Y. Pan, X. Hou, S.J. Weroha, R.J. Karnes, D. Wang, Q. Wu, D. Wu, H. Huang, DNA damage promotes TMPRSS2-ERG oncoprotein destruction and prostate cancer suppression via signaling converged by GSK3β and WEE1, Mol. Cell 79 (2020) 1008–1023, https://doi.org/10.1016/j.molcel.2020.07.028, e4.